STUDY OF BIOHEAT TRANSFER PROCESSES FOR HYPERTHERMIA CANCER TREATMENT

by

Mauricio Andrés Giordano

A thesis submitted in partial fulfillment of the requirements for the degree of

MASTER OF SCIENCE
in
MECHANICAL ENGINEERING

UNIVERSITY OF PUERTO RICO
MAYAGÜEZ CAMPUS
2009

Approved by:

_____	_____
Nellore Venkataraman, PhD Member, Graduate Committee	Date
_____	_____
Carlos Rinaldi, PhD Member, Graduate Committee	Date
_____	_____
Rubén Díaz Rivera, PhD Member, Graduate Committee	Date
_____	_____
Gustavo Gutiérrez, PhD President, Graduate Committee	Date
_____	_____
Basir Shafiq, PhD Representative of Graduate Studies	Date
_____	_____
Pablo Cáceres, PhD Chairperson of the Department	Date

ABSTRACT

Hyperthermia is a type of cancer treatment in which cancer cells are exposed to high temperatures (in the range 42-45°C). Research has shown that high temperatures can damage and kill cells by maintaining them in that range of temperatures for approximately thirty minutes. By killing cancer cells and damaging proteins and structures within them, hyperthermia may shrink tumors with minimal injury to normal tissues. In this research, the viability of the treatment is investigated by means of Pennes' bio-heat equation to model the heat diffusion in tissues for domains containing magnetic nanoparticles, which are the heat sources. The heating mechanism is the result of the magnetic relaxation of the particles (Brownian and/or Néel relaxation) by the application of alternating magnetic fields. The bio-heat equation is solved for different shapes of the domain and heating conditions by numerical and analytical methods. A method for solving analytically bio-heat problems by means of free-space Green's functions is developed and applied to some particular problems. A parametric analysis was carried out to develop the relative influence of the parameters involved in the process on the temperature profile, like the generation rate, perfusion rate and distribution of the sources. This study shows that with heating rates already achievable, it is possible to reach the therapeutic temperature profile. Then, the limitations in the treatment would rely in questions of toxicity, targeting, among others.

RESUMEN

Hipertermia es un tipo de tratamiento para el cáncer en el cual el tejido canceroso es sometido a altas temperaturas (en el rango 42-45°C). Estas altas temperaturas dañan e inducen la muerte celular luego de una exposición de alrededor de treinta minutos. De esta forma, el tratamiento por hipertermia puede reducir tumores con un daño leve al tejido sano colindante. La viabilidad del tratamiento es investigada modelando la difusión de calor en los tejidos a través del modelo de Pennes, conocido como bio-heat equation y usándolo para evaluar los perfiles de temperatura obtenibles en dominios de tejido conteniendo nanopartículas magnéticas de escala nanométrica, que son las fuentes de calor. Los mecanismos de generación son el resultado de efectos de relajación magnética (relajación Browniana y/o de Néel) bajo la acción de campos magnéticos alternos. La temperatura es resuelta para diferentes configuraciones del dominio y condiciones de generación por medio de técnicas analíticas y numéricas. En particular, se propone un método para resolver problemas de esta índole en medios infinitos y se muestra la aplicación del mismo a partir de unos casos particulares. Se llevo a cabo un análisis de la importancia relativa de los distintos parámetros que intervienen en el desarrollo del perfil de temperatura. Entre los parámetros analizados se encuentran la tasa de generación, la tasa de perfusión y la distribución de las fuentes. Este estudio muestra que, con las tasas de generación alcanzables actualmente, es posible establecer el perfil de temperatura terapéutico. Luego, limitaciones en la aplicación tendrían que ver con cuestiones como la toxicidad de las partículas, focalización, entre otras.

ACKNOWLEDGEMENTS

I would like to thank my advisor, Dr. Gustavo Gutierrez for giving me this opportunity and for the many things he did for me inside and outside the academic environment. I also want to express my gratitude to Dr. Carlos Rinaldi because he was also responsible for this chance of performing my master in the University of Puerto Rico.

To the members of my committee Dr. Carlos Rinaldi, Dr. Nellore Venkataraman and Dr. Ruben Diaz, thanks for your help and dedication.

I am very grateful to Dr. Luis E. Suarez for his invaluable help and friendship. Also I am grateful to Dr. Stefano Leonardi for his counseling and friendship.

I cannot reserve the acknowledgement to all the people that I have met along these years.

The Grant from NSF NIRT 0609117 provided the funding and the resources for the development of this research. At last, but the most important I would like to thank my family, friends and girlfriend, for their unconditional support, inspiration and love.

Table of Contents

Table List

Tables **Page**

Figure List

Figures **Page**

1 INTRODUCTION

1.1 Motivation

The survival rate for many types of cancer has improved in recent years; however, as the National Cancer Institute reports, cancer is still the second leading cause of death in the United States.

In contrast with chemotherapy and radiotherapy, the side effects of magnetic fluid hyperthermia are almost negligible. Assuming that the particles are not toxic, the patient could only feel soft arrhythmia. There is no pain involved and several applications of the magnetic field are possible without depositing more particles in the tissue.

Developing solutions for the temperature profiles achievable is mandatory for the treatment in order to be able to set the variables involved (concentration of particles, magnetic field intensity and frequency) to produce profiles that are close to the therapeutic one (see Figure 1.1) and, thus, specific to the cancerous tissues.

1.2 Importance of the Problem

Many efforts have been done in the last fifteen years to improve hyperthermia technique. Advances in the area of the nanotechnology have contributed to the development of the magnetic fluid hyperthermia which is very promising because, as it was addressed, it has fewer side effects than chemotherapy and radiotherapy that are the most used treatments for cancer. An exhaustive review of papers and an excellent description about the state of the art of hyperthermia is given by (Goya, Grazu et al. 2008).

There have been no trials in humans till now but, there are records for in vivo experiments (Jordan, Scholz et al. 1997; Moroz, Jones et al. 2002). The research group of Jordan in

Germany is the most advanced in the field and they have a prototype which is able to generate variables magnetic fields of intensity in the range 0 – 15 kA/m at the frequency of 100 kHz, and it has probes to invasively measure the temperature at real time to ensure that neither the upper limit of the therapeutic temperature threshold is exceed (this would result in thermal ablation) nor the lower limit is crossed, which would end up in under treatment. This prototype is capable to treat tumors placed in any region of the body.

Only local hyperthermia will be considered for magnetic fluid hyperthermia. In this case magnetic nanoparticles in a fluid carrier will be located inside the tumor through direct injection or arterial embolization, after which the tumor has to be exposed to a magnetic field. This field makes the particles to generate heat by magnetic relaxation mechanisms.

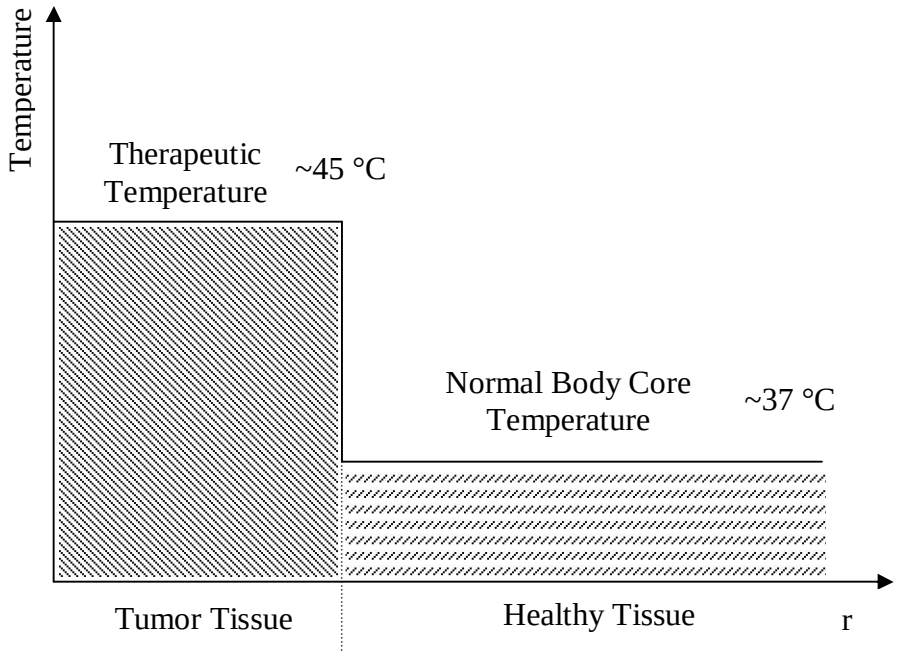

Figure 1.1: Ideal Therapeutic Temperature Profile

The above description of hyperthermia treatment shows the importance of knowing the temperature profile obtained under specific heating conditions. In that context, the ideal

temperature profile, as shown in Figure 1.1, is the one that maintaining the body temperature in healthy tissue also keeps constant the therapeutic temperature inside the tumor.

However, a smooth transition from the therapeutic temperature to the body temperature exists; in reality the profile is not flat, neither in the tumor nor in the normal tissue because of thermal diffusion.

1.3 Scope of the thesis

In the present research, the response of human tissue to heat deposition is analyzed taking care of the intrinsic mechanisms of thermoregulation, i.e. blood perfusion rate and metabolic heat generation. It is intended to get an answer for questions like: What is the necessary power dissipation required for the particles to produce the therapeutic temperature profile? Is the diffusion of the particles relevant to affect the heat diffusion? Is this Specific Absorption Rate (SAR) achievable? Is there a particular distribution for the particles that produces the closest temperature distribution to the ideal one? Knowing that the blood perfusion rate removes some of the heat produced for the particles, can this effect be neglected for the calculation of the temperature profile?

Regular domains in rectangular, cylindrical and spherical coordinate systems are considered and the temperature is solved by analytical, numerical and stochastic methods. The variations in the values of the thermo-physical properties of the tissues are negligible and, thus, neglected see Table 5.1.

1.4 Objectives

• To find an optimum achievable configuration of the system to produce the closest temperature profile to the therapeutic one.

• To determine whether the treatment can be successfully implemented from a thermal point of view.

• To show how analytic and numerical techniques can be used for solving bio-heat transfer problems.

• To get an insight of the mass and heat diffusion processes in living tissues.

1.5 Methodology

As was previously mentioned, numerical and analytical methods are used in this research to solve the Pennes' bio-heat model for different geometries, as well as, different spatial heating configurations and boundary conditions.

The analytical solutions are obtained using the Finite Fourier Transform (also known as Integral Transform) method and the Green's Function Method because they allow us to deal with time and space varying boundary conditions as well as time and space varying non homogeneous source terms. These analytical solutions are very useful for validating numerical codes and, also, to perform a sensitivity analysis of all the parameters that affect the thermal diffusion process. This analysis is valuable for revealing important information regarding the relative weight of the different processes that take place in the diffusion process.

Although elegant, the analytical methods, in general, are not suitable for solving the temperature field when the sources are randomly distributed along a certain region within the domain or when nonlinearities are present.

Regarding Green's functions, a method for infinitely large domains in rectangular, cylindrical and spherical coordinates is presented. The solutions obtained for such domains are called fundamental solutions or free space Green's function in literature. The integral transform method (Deen 1998; Ozisik 1968) is used for solving the case of a spherical tumor with the nanoparticles generating heat in its surface and the whole configuration surrounded by healthy tissue. Among the spatial heating considered, the following may be mentioned: point source, shell source, line source, plane source heat generation.

The bio-heat equation was solved numerically using a finite volumes approach. Also a Monte Carlo model was developed for the following reasons: It depends weakly on the dimension and the geometry of the domain; a computer code can be developed with certain ease; the method is intrinsically parallelizable because a random walk is independent from others allowing a reduction in computational time; the temperature of a point may be evaluated without solving the temperatures of all the point of the grid, which can be of particular interest in hyperthermia where the temperature in some isolated points is required.

The Finite Volumes method, is used to get an indirect validation of the solutions and gain confidence about them. A structured grid is constructed to mesh a cubic domain yielding a rather simple problem.

1.6 Organization of the Thesis

In chapter 2 a review of the fundamental concepts involved in the problem is presented along with the structure of the tissues, the features of tumor vasculature that make possible the treatment. Chapter 3 presents the mathematical formulation of the problem for the computation of the temperature profile with all the assumptions made and the initial and boundary conditions used. The methodology is depicted in Chapter 4, where the numerical and analytic methods used are developed in detail. Results and discussion that arises from them is exposed in Chapter 5. Conclusions are summarized and exposed in Chapter 6.

2 LITERATURE REVIEW

2.1 Definition of Transport Processes

For the problem in hand the transport processes involved are the heat diffusion and the mass diffusion. A brief review of these processes is presented in this section.

Two physical phenomena are involved in the transport of molecules: Diffusion and Convection (Truskey, Yuan et al.).

Diffusion is the random motion of molecules that arises from thermal energy transferred by molecular collisions. We can talk about heat diffusion or species diffusion (mass diffusion).

Convection, on the other hand, is a mechanism of transport resulting from the bulk motion of fluids.

2.1.1 Mass diffusion and Fick's Law

The relationship between the mass flux and the concentration gradient (known as a constitutive equation) was first quantified by Fick in 1855. Fick's law is strictly applicable to the diffusion in dilute binary solutions.

The quantity that relates the diffusion flux to the concentration gradient is the binary diffusion coefficient, D_{ij}, where the subscript *i* refers to the solute and *j* to the solvent. It is a function of the thermodynamic properties of the medium such as the temperature and the pressure and its magnitude depends upon the solute and the medium through which diffusion occurs.

Fick's law describes mass diffusion in tissues if the binary diffusion coefficient is replaced with an effective diffusion coefficient. This coefficient characterizes the diffusion of one

molecule relative to another. It incorporates the effect of increased diffusion distances and drag forces exerted by the extracellular matrix and cells (Truskey, Yuan et al.).

Information about the orders of magnitude of mass diffusion compared with heat diffusion is shown below using the Stokes-Einstein relation to estimate the mass diffusion coefficient for a dilute solution of the magnetic nanoparticles in tetradecane. The particles are assumed to be spherical and the surfactant layer is included in the radius.

The Stokes-Einstein relation provides a way to estimate the mass diffusion coefficient as the relation between the thermal energy of the system and the resistance to flow which is quantified through the translation tensor whose components are referred to as friction coefficients. For spherical particles, the information stored in the tensor can be reduced to a scalar, which is nothing but the Stokes solution for the drag coefficient for a spherical particle (Low-Reynolds number flow) $\mathrm{f} = 6\pi\mu R$.

Then, the diffusivity of species and the diffusivity of heat are given by:

$$D = \frac{k_B T}{\mathrm{f}} \left[\frac{m^2}{s}\right] = \frac{k_B T}{6\pi\mu R}\left[\frac{m^2}{s}\right] \tag{2.1}$$

$$\alpha = \frac{k}{\rho c} \left[\frac{m^2}{s}\right] \tag{2.2}$$

Where $k_B = 1.38\times10^{-23}\left[J/K\right]$ is the Boltzmann constant; T is the absolute temperature; μ is the dynamic viscosity of the carrier fluid; k is the thermal conductivity of tissue; ρ is the density of tissue; and c is the specific heat of tissue.

In order to get numerical values, the thermo-physical properties of tissue are used:

$$\rho = 1000\left[\frac{kg}{m^3}\right] \qquad k = 0.5\left[\frac{W}{mK}\right]$$

$$c_p = 3800\left[\frac{J}{kgK}\right]$$

Characteristics of the ferrofluid:

$$\mu = 0.00235\left[\frac{kg}{ms}\right] \qquad R = 30\ nm$$

For establishing the comparison between them their quotient is arranged, yielding

$$\frac{D}{\alpha} = \frac{k_B T / \mathrm{f}}{k / \rho c_P} = 2.3136\times10^{-6} \tag{2.3}$$

The result in equation (2.3) shows that the time scale for the mass diffusion is six orders of magnitude lower than the thermal diffusion.

This fact has two meaningful implications. First, there is no coupling in the equations and both diffusion processes can be regarded as independent from each other and the volume fraction of particles may be assumed to be a constant as well as the rate of heat generation; second, once the nanoparticles are placed inside the tumor they will stay there enough time for making subsequent magnetic field exposures without injecting more ferrofluid.

2.2 Drug Transport Within Solid Tumors

One of the main steps in magnetic fluid hyperthermia is the delivery of the magnetic nanoparticles. This justifies a review of the process of drug transport in tumors, as well as, to the structure of the blood vessel network through which they are going to be transported. In this context the word *drug* will be used for any agent that must be delivered in the treatment of cancer. These agents can be as small as an oxygen molecule or as large as immune cells.

In a tumor tissue, three different regions can be found. They are:

- Blood Vessles
- Interstitium
- Cells

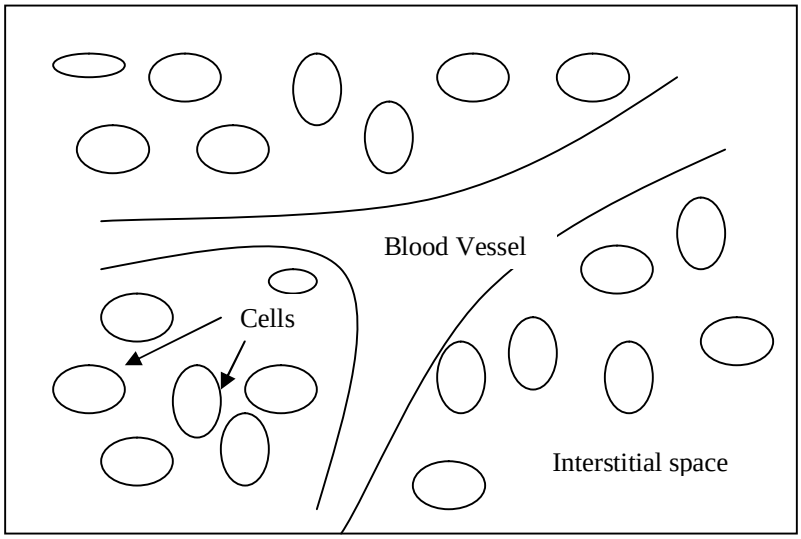

Figure 2.1: General Structure of Tissues at micro scale

There are significant differences in the way that these constituents are arranged in both types of tissues considered, healthy tissue and tumor tissue as it can be inferred from Table 2.1.

Table 2.1: Tumor tissue vs Normal tissue

	Solid Tumors	Normal Tissues
Volume fraction of blood vessels	0.01 to 0.28	0.019 to 0.3
Volume fraction of interstitial space	0.13 to 0.6	0.06 to 0.3

2.2.1 Tumor vasculature

Blood enters a normal organ through large arteries, which subsequently bifurcates into small arteries, arterioles, precapillary arterioles and capillaries (smallest blood vessels). Capillaries are responsible for nutrient and waste exchange between the blood and tissues.

In tumor vascular networks there is no such order, in other words the tumor vascular network is chaotic. Vessels division follows no pattern except for large arteries and veins that connect a tumor to the systemic circulation, structures in other vessels are heterogeneous and cannot be classified in any category.

Unique features appear in tumors that rarely occur in normal vasculature:

- Formation of vessel loops and shunts
- Bifurcation of a small vessels into two large ones
- Trifurcation of vessels

2.2.2 Tumor Microcirculation

Chaotic vasculature structure causes a heterogeneous blood flow, with velocity varying both spatially and temporally in a random manner. In some vessels, the direction of blood flow may even change with time (this is very unusual in normal tissues).

Some tumor vessels are too small that red blood cells cannot pass through and only plasma can enter this vessel which translates in a deficiency of oxygen inside tumor. This is one of the characteristics of solid tumors.

Blood flow determines how much of a drug systemically administrated can be delivered to a tumor. So improving tumor blood flow, the delivery of drugs to these regions will be

enhanced. Recall that, in this context, drug is used for any agent (nanoparticles) designated to the treatment of cancer.

2.2.3 Transvascular Transport

When drug molecules reach tumor microcirculation, they may cross the microvessel walls. The rate of transvascular transport is characterized by the microvascular permeability coefficient, which depends upon physical and chemical properties of the drug and properties of the vessel wall.

This permeability is heterogeneous in tumors and higher than that in normal tissues, the transport of macromolecules and nanoparticles is allowed.

The *cutoff pore size* in tumors can take values up to two microns when in normal tissues the maximum value for the pore size can be about 20 nanometers. This is the key of the magnetic fluid hyperthermia, therapeutic agents larger than 20 nm and smaller than the cutoff size of the pores of tumor vessels will accumulate preferentially in tumors.

2.2.4 Interstitial Transport

The interstitial space consists in interstitial fluid and extracellular matrix.

This type of transport is one of the most difficult steps in both, systemic and local drug delivery to tumor cells for the following reasons:

- Low convective transport due to elevated interstitial fluid pressure
- Outward gradients of the interstitial fluid pressure
- Large diffusion distances in some regions of the interstitium
- Binding of drugs to various components in tissues

2.3 Magnetically Mediated Hyperthermia

Experimental investigations of the application of magnetic materials for hyperthermia date back to 1957 when Gilchrist *et al* (Gilchrist RK 1957) heated various tissue samples with 20–100 nm size particles of γ -Fe_2O_3 exposed to a 1.2MHz magnetic field.

Since then, there have been numerous publications describing a variety of schemes using different types of magnetic materials, different field strengths and frequencies and different methods of encapsulation and delivery of the particles (Jordan, Scholz et al. 1999; Jordan, Scholz et al. 2001). In broad terms, the procedure involves dispersing magnetic particles throughout the target tissue, and then to apply an AC magnetic field of sufficient strength and frequency to cause the particles to heat by magnetic hysteresis losses or Neel relaxation (Hergt, Andra et al. 1998; Rosensweig 2002). This heat conducts into the immediately surrounding diseased tissue whereby, if the temperature can be maintained above the therapeutic threshold of 42˚C for 30 min or more, the cancer is destroyed.

The National Cancer Institute (www.nci.nih.gov) recognizes three different types of hyperthermia treatments:

1. *Local hyperthermia*: the heat is applied to a small area, such as a tumor, using various techniques that deliver energy to heat the tumor. Different types of energy may be used to apply heat, including microwave, radiofrequency, and ultrasound.
2. *Regional hyperthermia*: large areas of tissue, such as a body cavity, organ, or limb are heated using different approaches such as external applicators or regional perfusion.
3. *Whole body hyperthermia*: is used to treat metastatic cancer that has spread throughout the body.

The modality of cancer treatment referred in this work is a type of local hyperthermia which is called *magnetically mediated hyperthermia* or, more specifically, *magnetic fluid hyperthermia.*

Among all hyperthermia modalities including microwave, laser and ultrasonic wave-based treatments, magnetic fluid hyperthermia has the maximum potential for a selective targeting (between healthy and diseased cells), producing a lot less side effects than the well established treatments of chemotherapy and radiotherapy.

The magnetic fluid carrying the nanoparticles is delivered in one of these two ways (Moroz, Jones et al. 2002):

1. *Arterial embolization*: the fluid carrying the magnetic particles is injected in the arterial supply of the tumor and is used as the pathway to deliver them.
2. *Direct injection*: consists of directly injecting the fluid into the tumor tissue. The particles will be located in the interstitial space and, thus, when the magnetic field is then applied, the heat originates outside the cells.

In the research group, the nanoparticles are being synthesized with a coating with specific tumor antibodies so they are selectively ingested by the tumor cells, with minimal uptake by normal cells (differential endocytosis). Then, the time that the particles are going to be placed in the tumor region is increased which is very desirable in sight of future applications of the magnetic field.

2.4 Previous Work Using Pennes' Model

Bio-heat transfer processes in living tissues are often influenced by the effects of blood perfusion through the vascular network on the local temperature distribution. When there is a significant difference between the temperature of the blood and the tissue through which it

flows, convective heat transport will occur, altering the temperatures of both the blood and the tissue.

The blood/tissue thermal interaction is a function of several parameters including the rate of perfusion and the vascular anatomy, which vary widely among the different tissues, organs of the body, and pathology as discussed in the section 2.2. The literature contains an extensive compilation of perfusion rate data for many tissues and organs (Kreith F. 2000).

The rate of perfusion of blood through different tissues and organs varies depending on factors such as physical activity, physiological stimulus and environmental conditions.

There are several models of the bio-heat transfer; the first one was developed by (Pennes 1948) which is nothing but the heat diffusion equation with a term for the heat transport due to blood perfusion and another one to consider the metabolic heat generation. This model is applicable in tissues with small blood vessels. Other models were developed after Pennes' but the complexity of these models and the applicability of Pennes' equation in regions with small vessels make this model a good candidate for bio-heat studies. Most of the other models for bio-heat transfer are discussed in a rather exhaustive review in the work presented by (Arkin, Xu et al. 1994).

Several studies have aimed at obtaining analytical solutions to the Pennes' equation for a single region (Vyas and Rustgi 1992; Gao, Langer et al. 1995; Deng and Liu 2002). Other studies (Durkee, Antich et al. 1990 a; Durkee, Antich et al. 1990 b; Durkee and Antich 1991 a; Durkee and Antich 1991 b; Andra, d'Ambly et al. 1999) have shown work on analytical solutions for multi-layer regions. (Andra, d'Ambly et al. 1999) modeled the diseased tissue with constant heat generation by magnetic fluid hyperthermia as a finite spherical region surrounded by an infinite spherical region of healthy tissue. They neglected blood perfusion

effects in either region. (Durkee, Antich et al. 1990) modeled several finite regions in spherical and Cartesian coordinates with blood perfusion and constant heat generation. The inclusion of blood perfusion and modeling tissues as finite regions makes the model of Durkee et al. closer to reality. (Bagaria and Johnson 2005) modeled the diseased and healthy tissues as two finite concentric spherical regions and included the blood perfusion effect in both the regions. They have calculated analytical solutions to the model by separation of variables method and numerical solutions by an explicit finite differencing technique. Analytical and numerical solutions for cases with constant and spatially varying heat generation sources are presented in that work too. The model studies the proper distribution of magnetic particles throughout the tumor could minimize the damage to the surrounding healthy tissue while still maintaining a therapeutic temperature in the tumor. However, this distribution is defined mathematically but is not feasible to control in practical applications. A good discussion about the influence of the spatial generation in the temperature profile is done as well as of the influence of blood perfusion.

2.5 Heating Mechanisms in AC Magnetic Fields

(Rosensweig 2002) has studied the mechanism of heat generation in a magnetic fluid due to a variable magnetic field and, thus, developed dissipation relationships based on rotational relaxation of single domain magnetic particles dispersed in a liquid matrix. These particles are assumed to be less than 20nm in diameter so eddy current heating can be neglected.

In that work, Rosensweig found that there is strong size dependence in the heating rate. The size of the particle affect the time constant of each relaxation mechanism, the larger the particles the smaller Brownian relaxation time constant, otherwise, Neel relaxation

mechanism will dominate. This is due to that both mechanisms take place in parallel. In order to achieve high heating rates the Neel relaxation must not to be allowed to dominate.

The above mentioned power dissipation expression obtained by Rosensweig is widely used to model the power dissipation due to magnetic fluid during hyperthermia cancer treatment.

The mathematical formulation for the power dissipation is obtained performing an energy balance in an isolated sample, hence the increase in the internal energy of the isolated sample is the magnetic work:

$$\Delta U = -\mu_0 \oint M dH \tag{2.4}$$

Subjecting the sample to an alternating magnetic field of the form:

$$H_{(t)} = H_0 \cos(\omega t) = \mathrm{Re}[H_0 e^{i\omega t}] \tag{2.5}$$

Then, the magnetization is given by:

$$M_{(t)} = \mathrm{Re}[\chi H_0 e^{i\omega t}] \tag{2.6}$$

Where χ is the complex susceptibility: $\chi = \chi' - i\chi''$

Substitution of equations (2.5)-(2.6) in equation (2.4) yields:

$$\Delta U = 2\mu_0 H_0^2 \int_0^{2\pi/\omega} \sin^2(\omega t) dt \tag{2.7}$$

The power dissipation is given by the product of the increase in the thermal energy and the frequency of the magnetic field:

$$P = \mu_0 \pi \chi'' f H_0^2 \tag{2.8}$$

If each and every factor of the above equation is expressed in SI units *P* will be given in Joules per second or, equivalently, Watts. In this expression for the power dissipated was

assumed that the particles are single domain, all the processes are adiabatic and that eddy currents are negligible (due to the small size of the particles).

In order to make equation (2.8) useful, the out of phase component of the magnetic susceptibility must be related to the properties of the ferrofluid. This is done using the relaxation relationship developed by Shliomis (Shliomis 1974):

$$\frac{\partial M_{(t)}}{\partial t} = \frac{1}{\tau}(M_{0(t)} - M_{(t)}) \tag{2.9}$$

Where M_0 is the equilibrium magnetization. Replacing the expression for the real part of the complex magnetization in equation (2.9):

$$\chi^{"} = \frac{\omega\tau}{1+(\omega\tau)^2}\chi_0 \tag{2.10}$$

Substitution of equation (2.10) in equation (2.8) yields the expression that will be used to get the power loss of a ferrofluid:

$$P = \mu_0 \pi \chi_0 f H_0^2 \frac{2\pi f\tau}{1+(2\pi f\tau)^2} \tag{2.11}$$

Here, τ is the effective time constant, which can be obtained from the characteristic times for Brown and Neel relaxation processes:

$$\tau = \frac{\tau_B \tau_N}{\tau_B + \tau_N} \tag{2.12}$$

Where:

$$\tau_B = \frac{3\eta V_H}{kT} \tag{2.13}$$

$$\tau_N = \frac{\sqrt{\pi}}{2}\tau_0 \sqrt{\frac{k_b T}{\mathrm{K}V_M}} \tag{2.14}$$

η: viscosity of the carrier (liquid)

V_H: hydrodynamic volume

V_M: volume of the magnetic core

k_b: Boltzmann constant

T: absolute temperature

K: anisotropic constant

As it can be seen, the dependence of P, the power dissipated, as a function of the temperature is given through the time constants.

There is one equation remaining, and it has to do with that one for the equilibrium susceptibility which, with a conservative criterion, may be approximated using the susceptibility corresponding to the Langevin equation:

$$L_{(\xi)} = \frac{M}{M_s} = \coth\left(\frac{\xi - 1}{\xi}\right) \tag{2.15}$$

$$\xi = \mu_0 M_d \frac{HV_M}{kT}; \qquad M_s = \phi M_d \tag{2.16}$$

$$\chi_i = \left(\frac{\partial M}{\partial H}\right)_i = \mu_0 \phi M_d^2 \frac{V_M}{3kT} \tag{2.17}$$

The last equation can be obtained by differentiating the Langevin equation.

The frequency and strength of the externally applied AC magnetic field used to generate the heating is limited by deleterious physiological responses to high frequency magnetic fields. These include stimulation of peripheral and skeletal muscles, possible cardiac stimulation and arrhythmia, and non-specific inductive heating of tissue. Generally, the usable range of frequencies and amplitudes is considered to be $f = 0.05 - 1.2$ MHz and $H = 0 - 15$ kAm^{-1} (Pankhurst, Connolly et al. 2003). Experimental data on exposure to much higher frequencies

fields comes from (Atkinson, Brezovich et al. 1984) who developed a treatment system based on eddy current heating of implantable metal thermo seeds. Atkinson et al. concluded that exposure to fields where the product $H.f$ does not exceed 4.85x108 $Am^{-1}s^{-1}$ is safe and tolerable.

Even though much work has been done, there are still needs for better understanding of the influence of the spatial distribution of the sources in the temperature profile as well as the relationship between the volume fraction of particles and the heating rates achievable. Furthermore, few works have considered the incidence in the temperature distribution of changes in the blood perfusion coefficient.

3 MATHEMATICAL FORMULATION

3.1 Governing Equation

As it was mentioned in the introduction, a classical mathematical model for heat diffusion in biological bodies is used in this research. It was proposed by (Pennes 1948) and it is referred to it as the bio-heat equation. This equation is, basically, the result of performing an energy balance on a control volume in a stationary media assuming the domain as homogeneous and isotropic. This is an "effective model" which means that the whole domain is regarded to have effective thermal properties. In that work, Pennes, compared experimental data with the temperature predicted by the model, showing good agreement. The bio-heat equation assuming constant thermal properties and isotropic medium is:

$$(\rho c)_t \frac{\partial T_{(\mathbf{X},t)}}{\partial t} = k_t \nabla^2 T_{(\mathbf{X},t)} + (\rho c)_b \omega_b \left(T_a - T_{(\mathbf{X},t)}\right) + \dot{q}_{met(\mathbf{X},t)} + \dot{Q}_{gen(\mathbf{X},t)} \qquad (3.1)$$

Where:

T is the unknown tissue temperature °C

T_a is the arterial temperature °C

t subscript refers to tissue

b subscript b refers to blood

ρ is the density kg/m^3

c is the specific heat J/(kg °C)

ω_b is the blood perfusion coefficient 1/s

$\dot{q}_{met}$ is the rate of heat generation due to metabolism W/m^3

$\dot{Q}_{gen}$ represents the rate of heat generation due to the magnetic nanoparticles W/m^3

$\mathbf{X} = (x_1, x_2, x_3)$ are the spatial coordinates in any coordinate system m

In hyperthermia applications (T higher than T_a), the term containing the blood perfusion coefficient ω_b represents the heat removal produced by the flow of blood. It is a convection term in the differential equation whose effect is homogeneously distributed along the domain.

3.2 Initial and Boundary Conditions

The initial condition is assumed constant which would represent the core body temperature:

$$T_{(\mathbf{x},0)} = T_c \tag{3.2}$$

The numerical value of this temperature, T_c, can be regarded to be the same as the arterial temperature.

The adopted boundary conditions will depend on the case under consideration but whenever we are dealing with a bounded domain, they will be of Dirichlet type. The main reason for this choice is that the temperature field is solved in a relatively large domain compared to the tumor size which allows assuming that the temperature far from the sources (*i.e.* the nanoparticles inside the tumor tissue) is constant and equal to the body temperature.

So, the boundary condition is:

$$T_{(S_i,t)} = T_c \tag{3.3}$$

Where the subscript i= 1,2,3…,S_N denotes the boundary surface i of N boundary surfaces. As it was said, temperature is assumed constant on the boundary.

3.3 Equation in Dimensionless Form

Starting with the governing equation (3.1), by defining non-dimensional parameters, the equation will be reduced to non-dimensional form.

Defining the following non-dimensional parameters:

$$t^* = \frac{t\alpha}{L^2};\ x^* = \frac{x}{L};\ y^* = \frac{y}{L};\ z^* = \frac{z}{L} \tag{3.4}$$

$$\Theta_{\left(\eta_{(x)},\gamma_{(y)},\beta_{(z)},\tau_{(t)}\right)} = \frac{\left(T_{(x,y,z,t)} - T_a\right)}{T_a} \tag{3.5}$$

L is a characteristic length. The metabolic rate of heat generation $\dot{q}_{met}$ can change in a small interval of values and will be regarded as a constant throughout all this work.

The nanoparticles are modeled as point sources and it mathematical formulation in rectangular coordinates is given by $Q_{gen(x,y,z,t)} = P_{(x_0,y_0,z_0,t)}\delta_{(x-x_0)}\delta_{(y-y_0)}\delta_{(z-z_0)}$, where δ is the Dirac delta function and the difference in the argument means a displacement by x_0 units in the x-direction. The intensity of the sources is going to be considered as space-time independent $P_{(x_0,y_0,z_0,t)} = \text{constant}$.

Substituting equations (3.4) and (3.5) in (3.1):

$$\frac{\partial\Theta}{\partial t^*} = \nabla^{*2}\Theta - \frac{L^2}{k}\left(\rho c_P\right)_b \omega_b\Theta + \left(\dot{q}_{met} + \dot{Q}_{gen}\right)\frac{L^2}{T_a k} \tag{3.6}$$

Where $\nabla^* = L^2\left(\frac{\partial^2}{\partial x^{*2}} + \frac{\partial^2}{\partial y^{*2}} + \frac{\partial^2}{\partial z^{*2}}\right) = \frac{\partial^2}{\partial x^{*2}} + \frac{\partial^2}{\partial y^{*2}} + \frac{\partial^2}{\partial z^{*2}}$

From (3.6) dimensionless heat and perfusion terms: $q = \frac{\dot{q}_{met} L^2}{kT_a}$; $Q = \frac{\dot{Q}_{gen} L^2}{kT_a}$;

$\gamma^2 = \frac{L^2 (\rho c)_b \omega_b}{k}$ are defined.

Finally, by substitution in equation (3.6) we get a dimensionless form of the bio-heat equation:

$$\frac{\partial \Theta}{\partial t} = \nabla^2 \Theta - \gamma^2 \Theta + q + Q \tag{3.7}$$

Where the * was dropped in order to make the notation clearer. In equation (3.7), q represents the heat generated by metabolism; Q the heat generated by the magnetic nanoparticles; and the term with γ^2 is the one related with blood perfusion.

3.4 Assumptions

Since Pennes model for heat diffusion in tissues is going to be employed in this work, all the assumptions related with the transport process of this model apply here, and they can be summarized as:

- The rate of heat generation by tissue metabolism is constant.
- The volume flow of blood per unit volume is constant and uniform throughout the tissue which means a constant perfusion coefficient (ω_b).
- Effective thermo physical properties and temperature independent.

In the work by Pennes there are assumptions regarding the geometry of the forearm and the boundary conditions of that particular problem which are not needed here.

4 NUMERICAL AND ANALYTICAL APPROACHES

The mathematical model used in this work was proved to yield temperature profiles that are in good agreement with measurements of tissue temperature distributions as well as the model for the power dissipated by ferrofluids exposed to a time varying magnetic field.

In order to carry out an analysis that allows to confirm the viability of the magnetic fluid hyperthermia performing simulations can reduce considerably the number of experiments. In this way only few experiments are needed because the order of magnitude of the parameters involved in the treatment, *i.e.* magnetic field intensity and frequency, time of exposure, etc, may be set from the results obtained in these simulations.

4.1 Numerical Approaches

The application of the Monte Carlo and the Finite Volumes methods for bio-heat problems is developed in this section. The algorithms and the theoretical background for such methods are also addressed in some detail.

4.1.1 Monte Carlo Method

This method, also known as method of statistical trials, is a method of approximately solving problems using sequences of random numbers, which constitutes the core ingredient of the method. It is a means of treating mathematical problems, deterministic by nature, by *finding a probabilistic analog* and then obtaining approximate answers to this analog by some experimental sampling procedure. The solution of a problem by this method is closer in spirit to physical experiments than to classical numerical techniques (Haji-Sheikh 1966).

This method is very attractive because, in contrast to classical numerical methods, the efficiency depends weakly on the dimension and geometric details of the domain. The most outstanding feature of this method is that the solution can be addressed for a particular point within the domain without solving the entire temperature field, saving computational time. During hyperthermia treatment it is desirable to know the temperature at some particular regions inside and outside the tumor to ensure that under treatment is not going to occur. As the last justification for the choice of this fairly used method is that the inclusion of the point sources representing the generating magnetic nanoparticles is straightforward (Deng and Liu 2002), this idea will be seen clearly in the mathematical formulation and development of the algorithm.

As mentioned, an underlying concept of the probabilistic or Monte Carlo solution of differential equations is the random walk. A random walker may be regarded as a particle wandering within the domain according the probabilities established by the stochastic analog of the deterministic problem being solved. Different types of random walk lead to different Monte Carlo methods. The most popular types are the fixed-random walk and floating random walk. Other types, that are less popular, include the Exodus method, shrinking boundary method, inscribed figure method, and the surface density method (Sadiku 2001).

In the fixed-random walk method, the finite difference discretization of the governing equation is used in order to establish the probabilistic analog of the problem and is going to be used in this work. Here, the coefficients of the nodal temperatures define the probabilities for a random walker, situated in a certain node in the grid, to move in certain direction to a neighboring node. For instance, there will be four of these probabilities for a steady 2-D problem, and six for a steady 3-D one.

4.1.1.1 Discretized Governing Equation

An explicit formulation will be adopted but an implicit scheme can be adopted. For the sake of simplicity, a uniform grid is assumed where $\Delta x = \Delta y = \Delta z = \Delta$, so the discretized form of equation (3.1) is:

$$T_{(\mathbf{X},t)} = Fo\sum_{i=1}^{3} T_{(\mathbf{X}+\Delta\mathbf{X}_i,t)} + Fo\sum_{i=1}^{3} T_{(\mathbf{X}-\Delta\mathbf{X}_i,t)} + \left(1 - 6Fo - \frac{\left(\rho c_p\right)_b \omega_b \Delta t}{\left(\rho c_p\right)_t}\right) T_{(\mathbf{X},t)} + \frac{\dot{Q}_{(\mathbf{X},t)}\,\Delta t}{\left(\rho c_p\right)_t} \tag{4.1}$$

Where

Δt : time step

$Fo = \dfrac{\alpha \Delta t}{\Delta^2}$: Fourier number

ω_b : blood perfusion coefficient

$\mathbf{X} = (x_1, x_2, x_3)$: spatial coordinates

$\Delta\mathbf{X}_i$: displacement in the *i* direction

$\dot{Q}_{(\mathbf{X},t)} = \left(\rho c_p\right)_b \omega_b T_a + \dot{q}_{met} + \dot{Q}_{gen(\mathbf{X},t)}$: generalized heat sources

Re-writing equation (4.1) in the following form:

$$T_{(\mathbf{X},t)} = \frac{\left(\rho c_p\right)_t - \left(\rho c_p\right)_b \omega_b \Delta t}{\left(\rho c_p\right)_t} \left[\sum_{i=1}^{3} P_{\mathbf{X}_i^+} T_{(\mathbf{X}+\Delta\mathbf{X}_i,t)} + \sum_{i=1}^{3} P_{\mathbf{X}_i^-} T_{(\mathbf{X}-\Delta\mathbf{X}_i,t)} + P_0 T_{(\mathbf{X},t)} + \frac{\dot{Q}_{(\mathbf{X},t)}\,\Delta t}{\left(\rho c_p\right)_t} \right] \tag{4.2}$$

To get the equation (4.2), the common factor outside the square brackets was extracted from (4.1). The reason for doing so that a stochastic analog to the problem was being sought and it must satisfy the probability laws which, for this particular case are expressed by the following equations:

$$\sum_{i=1}^{3} P_{\mathbf{x}_i^+} + \sum_{i=1}^{3} P_{\mathbf{x}_i^-} + P_0 = 1 \tag{4.3}$$

$$P_{\mathbf{x}_i^+} = P_{\mathbf{x}_i^-} = \frac{Fo\left(\rho c_p\right)_t}{\left(\rho c_p\right)_t - \left(\rho c_p\right)_b \omega_b \Delta t} \geq 0 \tag{4.4}$$

$$P_0 = \left(1 - \frac{6Fo\left(\rho c_p\right)_t}{\left(\rho c_p\right)_t - \left(\rho c_p\right)_b \omega_b \Delta t}\right) \geq 0 \tag{4.5}$$

So the Monte Carlo model can be now established and the equation (4.2) may be given a probabilistic interpretation: if a random walking particle is instantaneously at the point (*x*, *y*, *z*), it has probabilities *Px+*, *Px−*, *Py+*, *Py−*, *Pz+* and *Pz−* of moving from (*x*, *y*, *z*) to (*x+Δ*, *y*, *z*), (*x−Δ*, *y*, *z*), (*x*, *y+Δ*, *z*), (*x*, *y−Δ*, *z*), (*x*, *y*, *z+Δ*), and (*x*, *y*, *z-Δ*) respectively; P_0 is the probability of the random walking particle not to move during that particular time step. It should be noticed that any of this actions implies one time step during the process of the random walk. In other words, if the temperature at a particular time t_f is needed, the time variable is set to this value and by the same time that the random walking process is taking place, the time starts to decrease in Δt units for each and every event. So, there are two ways in which a random walk could end; a) one boundary of the domain is reached; b) an initial point is reached, in other words, $t_f - m\Delta t = 0$, where *m* is a variable which count for the number of steps of the random walker in the grid for that particular random walk.

If the lower limit for the inequality (4.5) is chosen, the value for the time step is set as $\Delta t = \left(1 - 6Fo\right)\frac{\left(\rho c_p\right)_t}{\left(\rho c_p\right)_b \omega_b}$ the probability for the random walker to stay in the same grid point is zero, *i.e.* $P_0 = 0$, and the walker would move in the grid in each time step.

4.1.1.2 Formulation of the Algorithm

In order to develop a computer code it is necessary to relate the movement of the random walking particle with the probabilities of the model. This is done by generating pseudo random numbers between zero and one and instructing the particle to walk according the cumulative probabilities:

$$\begin{aligned}
&(x,y,z)\rightarrow(x+\Delta,y,z) && \text{if } 0\le RN<P_{\mathbf{x}_1^+}\\
&(x,y,z)\rightarrow(x,y+\Delta,z) && \text{if } P_{\mathbf{x}_1^+}\le RN<P_{\mathbf{x}_1^+}+P_{\mathbf{x}_2^+}\\
&(x,y,z)\rightarrow(x,y,z+\Delta) && \text{if } P_{\mathbf{x}_1^+}+P_{\mathbf{x}_2^+}\le RN<P_{\mathbf{x}_1^+}+P_{\mathbf{x}_2^+}+P_{\mathbf{x}_3^+}\\
&(x,y,z)\rightarrow(x-\Delta,y,z) && \text{if } P_{\mathbf{x}_1^+}+P_{\mathbf{x}_2^+}+P_{\mathbf{x}_3^+}\le RN<P_{\mathbf{x}_1^+}+P_{\mathbf{x}_2^+}+P_{\mathbf{x}_3^+}+P_{\mathbf{x}_1^-}\\
&\quad\mathbb{M}\qquad\mathbb{M} && \qquad\mathbb{M}\\
&(x,y,z)\rightarrow(x,y,z) && \text{if } 1\text{-}P_0\le RN\le 1
\end{aligned} \tag{4.6}$$

Where *RN* means Random Number.

If the interest is to solve for the temperature of the arbitrary grid point (*x*,*y*,*z*), *N* random walking particles must be dispatched from this point. Each particle will wander through the grid of the domain till either a boundary or an initial point is reached, *i.e.*, a point within the domain when the time variable value is zero.

Now, an stochastic variable ξ can be defined, whose expectation will be the approximation to the temperature for the point where the random walking particles have started:

$$\xi_j=\sum_{i=1}^{k-1}\left(\frac{\left(\rho C_p\right)_t-\left(\rho C_p\right)_b\omega_b\Delta t}{\left(\rho C_p\right)_t}\right)^{i+1}\frac{\dot{Q}\Delta t}{\left(\rho C_p\right)_t-\left(\rho C_p\right)_b\omega_b\Delta t}+\left(\frac{\left(\rho C_p\right)_t-\left(\rho C_p\right)_b\omega_b\Delta t}{\left(\rho C_p\right)_t}\right)^{k}f_{(G)} \tag{4.7}$$

The subscript *j* refers to each random walk, *i* refers to each step of the random walking particle, *k* to the last step and G may be either a boundary point, $S_l, l=1,2,.....,N$, or an

initial point so the value of $f_{(G)}$ will be either a boundary temperature (Dirichlet boundary condition) or the initial temperature of the point where the particle was stand in whether the boundary was reached or time variable was zero, respectively. Recall that $\dot{Q}_{(\mathbf{x},t)} = \left(\rho c_p\right)_b \omega_b T_a + \dot{q}_{met} + \dot{Q}_{gen(\mathbf{x},t)}$ includes all the sink/source terms.

Table 4.1: Tallies for the Monte Carlo Method

CONDITION	TALLY
BOUNDARY POINT	$T_{(S_l,t)}$
INITIAL POINT	$T_{(\mathbf{x},t=0)}$
METABOLIC HEAT GENERATION	$\dfrac{\dot{q}_{met}\,\Delta t}{\left(\rho C_p\right)_t - \left(\rho C_p\right)_b \omega_b \Delta t}$
PERFUSION	$\dfrac{\left(\rho C_p\right)_b \omega_b T_a \Delta t}{\left(\rho C_p\right)_t - \left(\rho C_p\right)_b \omega_b \Delta t}$
NANOPARTICLES HEAT GENERATION	$\dfrac{\dot{Q}_{gen(\mathbf{x},t)}\,\Delta t}{\left(\rho C_p\right)_t - \left(\rho C_p\right)_b \omega_b \Delta t}$

As the particle wanders through the grid nodes the term corresponding to the metabolic heat must be tallied, as well as that one corresponding to the heat removal associated with blood perfusion. The generating particles are modeled as point heat sources whose power dissipation is regarded to be constant. This means that the effect of these point sources is taken into account only when the random walking particle steps on one of the nodes where a particle is located.

Finally, the temperature at the point $\mathbf{X}_0 = (x_0, y_0, z_0)$ at time t_0 is approximated after the Nth random walk by:

$$T_{(\mathbf{x}_0, t_0)} = \frac{1}{N} \sum_{j=1}^{N} \xi_j \tag{4.8}$$

4.1.2 Finite Volumes

The first step in solving a differential equation using the finite volume method is to perform a discretization of the domain in little volumes called finite volumes as shown in Figure 4.1. In this figure the dashed lines represent the contour of the finite volumes. Inside each of these volumes a node is placed where the function, in this case the temperature, is going to be determined.

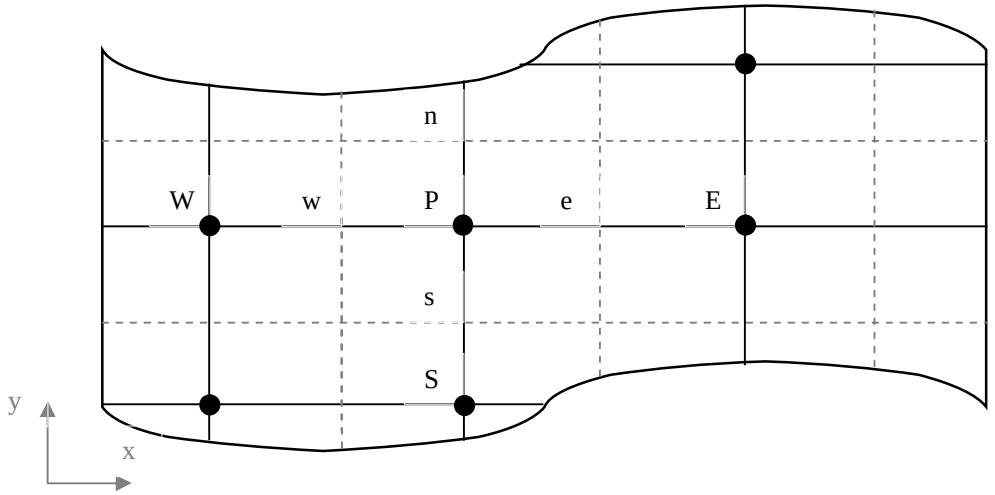

Figure 4.1: 2-D grid and notation used

In the notation commonly used (geographic notation), the capital letters are reserved for the nodes or grid points and small letters are reserved for control volume faces as shown in Figure 4.1. In this notation, P is the center of the control volume. The letters N, S, E, W, T, B denote North, South, East, West, Top and Bottom respectively. In the figure T and B are not

visualized. This is the most used notation for the finite volume method; it is used in (Patankar 1980; Versteeg and Malalasekra 1995; Ferziger and Peric 2002).

The second step is to discretize the equation along with the linearization of the non-homogeneous terms (if necessary), after which a set of linear equations in terms of the nodal temperatures is obtained.

Finally, using a linear solver, iterative or direct depending upon the size of the system, the unknown temperatures are determined.

4.1.2.1Discretization of the Governing Equation

Equation (3.7) is rewritten here but with $q+Q= H$, including all the heat sources

$$\frac{\partial \Theta}{\partial \tau} = \nabla^2 \Theta - \gamma^2 \Theta + H \tag{4.9}$$

Where the Laplacian is in terms of the dimensionless spatial coordinates.

In order to get the discretized form of this equation, integration along an arbitrary control volume followed by integration over a time step are carried out. This approach is what distinguishes the finite volume method from other methods for solving partial differential equations; it represents a flux balance of the property (temperature, in this case) over each and every control volume in each time step, exposing the programmer to the underlying physical concepts of the problem at hand during the formulation.

Then, the integral over a control volume is discretized as

$$\int_{\Delta V} \frac{\partial}{\partial x}\left(\frac{\partial \Theta}{\partial x}\right) dxdydz = A_e\left(\frac{\partial \Theta}{\partial x}\right)_e - A_w\left(\frac{\partial \Theta}{\partial x}\right)_w \tag{4.10}$$

Now, it is necessary to relate the flux at the control volume faces with the nodal values of Θ. This is done by approximating the spatial derivatives through the grid point values by means of the incremental quotient:

$$\left(\frac{\partial\Theta}{\partial x}\right)_e = \left(\frac{\Theta_E - \Theta_P}{\delta x_{PE}}\right) \tag{4.11}$$

Before taking this results to equation (4.9), it is necessary to discretize the time derivative. If it is assumed that the nodal temperatures prevails over the entire control volumes:

$$\int_{CV}\left[\int_t^{t+\Delta t}\frac{\partial\Theta}{\partial t}dt\right]dV = \left(\Theta_P - \Theta_P^o\right)\Delta V \tag{4.12}$$

Where the superscript "o" refers to nodal temperature at time level *t*.

Integrating over a control volume and linearizing the source term:

$$\int_{CV} H dV = \bar{S}\Delta V = S_p\Theta_P + S_u \tag{4.13}$$

The bar over *S* means that it is an averaged value of the generation in all the control volume.

Substituting equations (4.10-4.13) in equation (4.9)

$$\begin{aligned}\left(\Theta_P - \Theta_P^o\right)\Delta V = \int_t^{t+\Delta t}\Bigg[&A_e\left(\frac{\Theta_E - \Theta_P}{\delta x_{PE}}\right) - A_w\left(\frac{\Theta_P - \Theta_W}{\delta x_{WP}}\right) + A_n\left(\frac{\Theta_N - \Theta_P}{\delta y_{PN}}\right) - \\ &A_s\left(\frac{\Theta_P - \Theta_S}{\delta y_{SP}}\right) + A_t\left(\frac{\Theta_T - \Theta_P}{\delta z_{PT}}\right) - A_b\left(\frac{\Theta_P - \Theta_B}{\delta z_{BP}}\right)\Bigg]dt + \int_t^{t+\Delta t}\bar{S}\Delta V dt\end{aligned} \tag{4.14}$$

An assumption about the variation of the temperature with time is now needed. It may be used the values for the temperatures at *t* or *t+Δt* or another weighted combination of both leading to the different integration schemes. The fully implicit, *i.e. t+Δt,* scheme is used here because its robustness and unconditional stability. This stability is guaranteed for any size of the time step because all the coefficients are positive, for a more detailed explanation see

(Versteeg and Malalasekra 1995) chapter 5. Although the stability is assured, large time steps should be avoided because the accuracy of this scheme is first order in time. In order to get good accuracy, the time step (for a uniform grid and constant conductivity) is maintained approximately in the order of $\frac{\Delta x}{6}$. Recall that all the variables involved here are dimensionless, this is why the thermal diffusivity does not appear explicitly.

Using the fully implicit discretization, the equation for each interior grid point is:

$$a_P\Theta_P = a_E\Theta_E + a_W\Theta_W + a_N\Theta_N + a_S\Theta_S + a_T\Theta_T + a_B\Theta_B + a_P^o\Theta_P^o + S_u \tag{4.15}$$

The values for each of the coefficients appearing in (4.15) are summarized in the Table 4.2.

Table 4.2: Finite Volumes Coefficients for Interior Nodes

a_I	a_P	S_p	S_u
$\frac{A_i}{\delta_{PI}}$	$a_P^o + \sum_I a_I - S_P$	$-\gamma^2\Delta V$	$\left(q_{met} + Q_{gen}\right)\Delta V$

Corrections in S_p, S_u and, hence, a_P must be carried out for the boundary nodes. In the case of Dirichlet boundary conditions, the type for the problem in hand, a prescribed temperature is set to all the nodes at a boundary. Then, the corresponding term in equation (4.15) can be evaluated and it will be included in S_u for the equation of that node.

After an equation like (4.15) is derived for each and every interior grid point, a linear system of N equations is obtained whose unknowns, as previously mentioned, are the temperatures of the grid nodes.

4.1.2.2 Algorithm for Solving the Linear System of Equations

For solving the linear system produced by the discretization of the dimensionless governing equation, the Bi-Conjugate Gradient Stabilized (BCGSTAB) method was chosen, mainly for its fast convergence and stability.

This method is a modification to the Conjugate Gradient (CG) method in order to make it suitable for solving nonsymmetric linear systems. The BCGSTAB is like applying the CG (applicable to symmetric matrices) to an augmented matrix constructed as shown in equation (4.16).

$$\text{Augmented Matrix} = \begin{bmatrix} A & 0 \\ 0 & A \end{bmatrix} \tag{4.16}$$

For this work, the algorithm provided by Ferziger and Peric (Ferziger and Peric 2002) was modified and employed (Gutierrez 2002).

4.1.2.3 Grid Generation

The grid generated in the domain has the following features:

- It is uniform: the point sources modeling the nanoparticles appear as generating finite volumes in the code. In order to be consistent, the energy released from these finite volumes must be equal to that released by the magnetic nanoparticles. It is common to make a grid refinement around each source for the sake of accuracy. However this would result in a nonuniform grid. Because the solver being used in the code (CGSTAB) is very efficient, there is no need to break the uniformity of the grid, instead the size of the control volumes is made small enough to get a good accuracy.

- The grid independence was reached after reducing the size of the volumes till the results stoped changing. This procedure is necessary to make sure that the algorithm converges to the solution.

The domain's shape does not change, i.e. it is time independent, so the grid is constructed once and needs not to be updated.

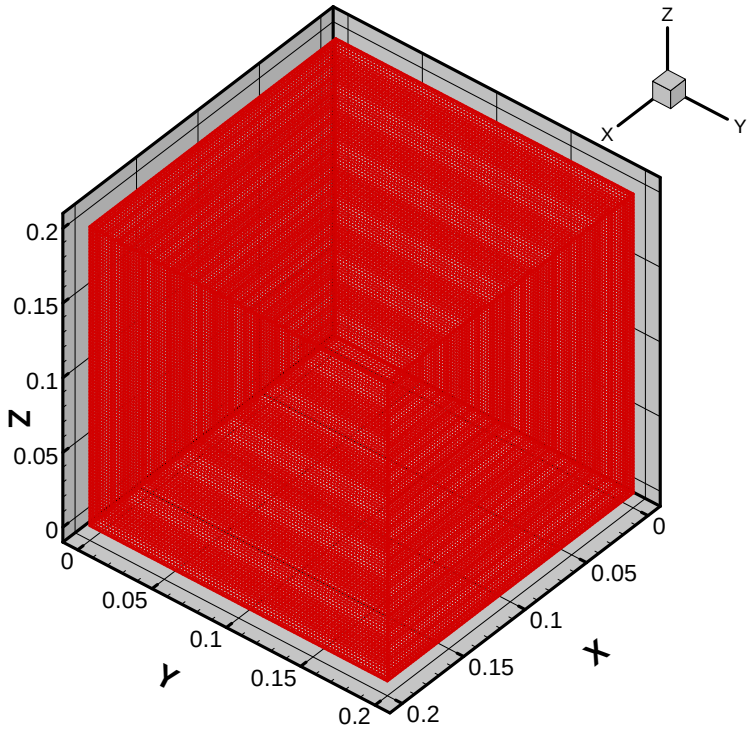

Figure 4.2: Grid for the Finite Volumes Method

4.2 Analytical Approaches

In order to gain some insight in the order of magnitude of the response of the system to the heating rates achievable and also the transient response, analytical solutions are very useful. Unfortunately, if point sources are randomly distributed in the domain, the problem is out of the scope of analytical methods, in general. Beside this, some configurations of the domain, boundary conditions and spatial heating lead to a problem exhibiting some type of symmetry

reducing the number of coordinates and yielding a problem suitable to be solved by means of the analytical methods used in this work.

In the following two sections a discussion of the analytical methods that are used is presented and the results for particular configurations are shown in the next chapter.

4.2.1 Green's Function Approach

The Green's function method for solving linear differential equations is based in the main feature of a linear system, *i.e.* the superposition principle.

The Green's function for a given partial differential equation and corresponding initial and boundary conditions is the response of the system by the action of a unit instantaneous impulse acting in an arbitrary point r at an arbitrary time τ. By the term instantaneous is meant that the source (in this particular case, the heat source) releases all its heat spontaneously at a time τ in a point r' within the domain. In other words, it is the solution, G, to a partial differential equation defined by the same linear operator than that of the original problem where the non homogeneity of the differential equation is an instantaneous point source of unit strength and the initial and boundary conditions are the homogeneous version of the boundary conditions of the original problem.

Thus, a Green's function is like a block containing the information regarding the response of a system to an instantaneous point impulse (in this context the impulse is a heat pulse). Then, any other type of forcing term can be thought as the combined effect of many impulses and, thus, the solution can be obtained in this way by a convolution integral. The mathematical form of the Green's function depends upon the coordinate system adopted, the linear differential operator and the boundary conditions.

There already is a rather exhaustive data base, *e.g.* (Beck, Cole et al. 1992), of Green's functions for the heat diffusion equation in the most commonly used orthogonal coordinate systems and for the three major types of boundary conditions. In order to this data base be useful for bio-heat diffusion problems a transformation is employed to the governing equation so that, after this transformation, the equation reads like the former with an additional factor in the non-homogeneous terms of the equation.

Starting with the governing equation written as given by equation (3.7):

$$\frac{\partial \Theta}{\partial t} = \nabla^2 \Theta - \gamma^2 \Theta + H \tag{4.17}$$

And defining $\Theta_{(\mathbf{X},t)} = W_{(\mathbf{X},t)} e^{-\gamma^2 t}$, after substitution yields:

$$\frac{\partial W}{\partial t} = \nabla^2 W + H e^{\gamma^2 t} \tag{4.18}$$

Which is the heat diffusion equation, where $H = q + Q$ includes all the heat sources, due to metabolism and particles. Note that, for convenience of notation, τ was replaced by t in equation (3.7).

The Green's function for the equation (4.18) plus suitable boundary conditions will be the solution of the auxiliary problem subjected to the homogeneous version of the same type of boundary conditions:

$$\frac{\partial G}{\partial t} = \nabla^2 G + \delta_{(\mathbf{x}-\mathbf{x}')} \delta_{(t-\tau)} \tag{4.19}$$

δ is the Dirac delta function.

As it was already stated, provided we have the Green's function of a particular problem, the temperature distribution is obtained by means of the Green's function solution equation whose derivation is omitted (see (Ozisik 1980) for details):

$$\Theta_{(\mathbf{x},t)} = \Theta_{in(\mathbf{x},t)} + \Theta_{g(\mathbf{x},t)} + \Theta_{b.c.(\mathbf{x},t)} \tag{4.20}$$

$$\Theta_{in(\mathbf{x},t)} = \int_R G_{(\mathbf{x},t|\mathbf{x}',0)} F_{(\mathbf{x}')} dV' \tag{4.21}$$

$$\Theta_{g(\mathbf{x},t)} = \int_{\tau=0}^{t} \int_R G_{(\mathbf{x},t|\mathbf{x}',\tau)} H_{(\mathbf{x}',\tau)} dV' d\tau \tag{4.22}$$

$$\Theta_{b.c.(\mathbf{x},t)} = \int_{\tau=0}^{t} \sum_{i=1}^{s} \int_{S_i} f_{i(\mathbf{x}_i',\tau)} G_{(\mathbf{x},t|\mathbf{x}_i',\tau)} ds_i' d\tau - \int_{\tau=0}^{t} \sum_{j=1}^{s} \int_{S_j} f_{j(\mathbf{x}_j',\tau)} \left. \frac{\partial G}{\partial n_j'} \right|_{\mathbf{x}=\mathbf{x}_j'} ds_j' d\tau \tag{4.23}$$

The subscript *in* in the general solution (4.20) refers to the effect of the initial condition, *g* to the generation effect and *b.c.* to the effect of boundary conditions. $F_{(\mathbf{x}')}$ in (4.21) represents an arbitrary initial condition. The two terms in the contribution of the boundary conditions are for the boundary conditions of second (Neumann) and third (Robin) kind, for boundary conditions of the first kind (Dirichlet) respectively. $f_{i(\mathbf{x}_i',\tau)}$ is the non homogeneity of the boundary condition. The summations are performed over each and every boundary surface s_i, i= 1,2,3,… S and the tilde is for denoting a dummy variable. The n_j in the expression for the boundary condition of first time refers to the normal outward direction of the j boundary surface.

In the following sections the solution to the bio-heat equation for point, line and plane sources in unbounded domains are developed by using the Green's function method developed here. These Green's functions are called fundamental, principal or free space Green's functions and they were not reported in the literature until now.

4.2.2 Free-Space Green's Function for the Bio-Heat Operator

For obtaining the Green's functions, an equation like

$$L\left(G_{(\mathbf{x},t)}\right)=\delta_{(\mathbf{x}-\mathbf{x}_0)}\delta_{(t-\tau)} \tag{4.24}$$

Must be solved, where *G* is the Green's function. Depending on the geometry and boundary conditions, there are many expressions for the Green's function for a particular linear differential operator, e.g. *L*. Then, it is useful to split the Green's function in two parts:

$$G=U+h \tag{4.25}$$

Where *U* is a particular solution, also called free-space Green's function, which need not satisfy the boundary conditions associated with equation (4.24), while *h* is a solution of the homogeneous equation $L(G)=0$ but with boundary conditions such that the superposition $U+h$ does, indeed, satisfy the boundary conditions for the original Green's function problem defined by equation (4.24).

In the following sub-sections the mathematical formulation of the free-space Green's function problem for the bio-heat operator is set for rectangular, cylindrical and spherical coordinate systems. All the formulation is developed using the dimensionless form of the governing equation, shown in chapter 3.

4.2.2.1 Cartesian Coordinates

The fundamental solution *U* for a one dimensional problem in Cartesian coordinates is the solution of the dimensionless equation:

$$L(U)=\left(\frac{\partial}{\partial t}-\frac{\partial^2}{\partial x^2}+\gamma^2\right)U=\delta_{(x-x')}\delta_{(t-\tau)} \tag{4.26}$$

The Fourier transform with respect to the spatial coordinate is used for eliminate the spatial variable and then an ordinary equation in time must be solved. The notation and the mathematical form used here for the transform and its inverse are:

$$\Im\left\{U_{(x,t)}\right\}=\hat{U}_{(\omega,t)}=\frac{1}{\sqrt{2\pi}}\int_{-\infty}^{\infty}U_{(x,t)}e^{-i\omega x}dx \tag{4.27}$$

$$U_{(x,t)}=\Im^{-1}\left\{\hat{U}_{(\omega,t)}\right\}=\frac{1}{\sqrt{2\pi}}\int_{-\infty}^{\infty}\hat{U}_{(\omega,t)}e^{i\omega x}d\omega \tag{4.28}$$

So, taking the Fourier transform to both sides of equation (4.26):

$$\frac{\partial\hat{U}}{\partial t}+\left(\omega^2+\gamma^2\right)\hat{U}=\frac{\delta_{(t-\tau)}}{\sqrt{2\pi}}e^{-i\omega x'} \tag{4.29}$$

Note that the right hand side of equation (4.29) is zero for either $t<\tau$ or $t>\tau$, so we have two conditions for $\hat{U}$:

$$\hat{U}=\begin{cases}Ae^{-\left(\omega^2+\gamma^2\right)t} & \text{for } t<\tau\\ Be^{-\left(\omega^2+\gamma^2\right)t} & \text{for } t>\tau\end{cases} \tag{4.30}$$

In order to relate the both solutions in (4.30) and to incorporate the singularity in produced by the Dirac delta, integration is performed in (4.29) with respect to *t* from $\tau-\varepsilon$ to $\tau+\varepsilon$ being ε as small as desired. This yield, in the limit when $\varepsilon\to 0$:

$$-Ae^{-\left(\omega^2+\gamma^2\right)\tau}+Be^{-\left(\omega^2+\gamma^2\right)\tau}=\frac{e^{-i\omega x'}}{\sqrt{2\pi}} \tag{4.31}$$

On the other hand, from (4.26) we have $U=0$ if $t<\tau$, then $\hat{U}=0$ and $A=0$ from (4.30). In this way $B=e^{-i\omega x'+\left(\omega^2+\gamma^2\right)\tau}\Big/\sqrt{2\pi}$ and replacing in (4.30):

$$\hat{U}=\frac{e^{-i\omega x'-\left(\omega^2+\gamma^2\right)(t-\tau)}}{\sqrt{2\pi}} \qquad \text{for } t>\tau \tag{4.32}$$

Taking the Fourier inverse transform, the so called principal or free space solution for the bio-heat differential operator, *U*, is obtained:

$$U = \frac{H_{(t-\tau)} e^{-\gamma^2 (t-\tau)}}{2\pi} \int_{-\infty}^{\infty} e^{-i\omega(x-x')-\omega^2(t-\tau)} d\omega \tag{4.33}$$

Performing the integration:

$$\boxed{U_{(x,t|x',\tau)} = \frac{H_{(t-\tau)}}{\sqrt{4\pi(t-\tau)}} e^{\left[\frac{-(x-x')^2}{4(t-\tau)} - \gamma^2(t-\tau)\right]}} \tag{4.34}$$

Where $H_{(t-\tau)}$ is the Heaviside unit step function.

This is the first of the three fundamental solutions for the bio-heat linear differential operator.

4.2.2.2 Cylindrical Coordinates

Following the same procedure used to derive the solution in Cartesian coordinates, it is possible to find the free-space solution for the bio-heat differential operator in cylindrical coordinates. The equation (dimensionless) to be solved is:

$$L(U) = \left(\frac{\partial}{\partial t} - \frac{\partial^2}{\partial r^2} + \frac{1}{r}\frac{\partial}{\partial r} + \gamma^2 \right) U_{(r,t|r',\tau)} = \frac{\delta_{(r-r')}\delta_{(t-\tau)}}{2\pi r} \tag{4.35}$$

The Hankel transform is going to be used to transform the *r* variable. For an arbitrary function *f(x)* it is defined as:

$$\overline{f}_{(\lambda)} = \int_{x=0}^{\infty} f_{(x)} J_{o(\lambda x)} x dx \tag{4.36}$$

$$f_{(x)} = \int_{\lambda=0}^{\infty} \overline{f}_{(\lambda)} J_{0(\lambda r)} \lambda d\lambda \tag{4.37}$$

Where $J_{0(\lambda x)}$ is the Bessel function of first kind, order zero and argument (λx).

Taking the Hankel Transform to (4.35)

$$\frac{\partial \overline{U}}{\partial t} + \left(\lambda^2 + \gamma^2\right)\overline{U} = \frac{J_{0(\lambda r')}\delta_{(t-\tau)}}{2\pi} \tag{4.38}$$

Noticing that the right hand side of equation (4.35) is zero for $t > \tau$ and $t < \tau$, the solution for those intervals is:

$$\bar{\bar{U}} = \begin{cases} Ae^{-\left(\lambda^2+\gamma^2\right)t} & \text{for } t > \tau \\ Be^{-\left(\lambda^2+\gamma^2\right)t} & \text{for } t < \tau \end{cases} \tag{4.39}$$

Integrating (4.38) from $\tau - 0$ to $\tau + 0$

$$Ae^{-\left(\lambda^2+\gamma^2\right)\tau} - Be^{-\left(\lambda^2+\gamma^2\right)\tau} = \frac{J_{0(\lambda r')}}{2\pi} \tag{4.40}$$

As another relation, recall that *U*, and hence $\bar{\bar{U}}$, is zero for $t < \tau$, so *B*=0. Then

$$A = \frac{J_{0(\lambda r')}}{2\pi} e^{\left(\lambda^2+\gamma^2\right)\tau} \tag{4.41}$$

And

$$\bar{\bar{U}} = \frac{J_{0(\lambda r')}}{2\pi} e^{-\left(\lambda^2+\gamma^2\right)(t-\tau)} \tag{4.42}$$

Finally, taking the inverse Hankel Transform:

$$U = \int_{\lambda=0}^{\infty} \bar{\bar{U}} J_{0(\lambda r)} \lambda d\lambda = \frac{1}{2\pi} \int_{\lambda=0}^{\infty} e^{-\left(\lambda^2-\gamma\right)(t-\tau)} J_{0(\lambda r)} J_{0(\lambda r')} \lambda d\lambda \tag{4.43}$$

The integral $\int_{\beta=0}^{\infty} \beta e^{-\beta(t-\tau)} J_{0(\beta r)} J_{0(\beta r')} d\beta$ can be integrated analytically (Erdelyi, Magnus et al. 1954):

$$\int_{\lambda=0}^{\infty} e^{-\lambda^2(t-\tau)} J_{0(\lambda r)} J_{0(\lambda r')} \lambda d\lambda = \frac{1}{2\left(t-\tau\right)} e^{-\frac{\left(r^2+r'^2\right)}{4(t-\tau)}} I_0\left(\frac{rr'}{2\left(t-\tau\right)}\right) \tag{4.44}$$

The final expression for *U* is given by

$$U_{(r,t|r',\tau)} = \frac{H_{(t-\tau)}}{2(t-\tau)} e^{-\frac{\left(r^2+r'^2\right)}{4(t-\tau)}-\gamma^2(t-\tau)} I_0\left(\frac{rr'}{2(t-\tau)}\right) \tag{4.45}$$

$I_{0(rr'/2(t-\tau))}$ is the modified Bessel's function of first kind, order zero and argument $rr'/2(t-\tau)$.

The 2π of the denominator was dropped so that this result for U can be directly used in the Green's function solution equation.

This is the second fundamental solution for the bio-heat linear differential operator, corresponding with cylindrical coordinates. The domain is unbounded in the *z* and *r* directions.

4.2.2.3 Spherical Coordinates

The equation for the principal solution, *U*, in spherical coordinates reads like:

$$L(U) = \left(\frac{\partial}{\partial t} - \frac{\partial^2}{\partial r^2} - \frac{2}{r}\frac{\partial}{\partial r} + \gamma^2\right) U = \frac{\delta_{(r-r')}\delta_{(t-\tau)}}{4\pi r^2} \tag{4.46}$$

In order to solve this problem, first, a transformation $U = \frac{\Phi}{r} e^{-\gamma^2 t}$ is carried out and equation (4.46) transforms to:

$$\frac{\partial \Phi}{\partial t} = \frac{\partial^2 \Phi}{\partial r^2} + \frac{e^{\gamma^2 t}}{4\pi r}\delta_{(r-r')}\delta_{(t-\tau)} \tag{4.47}$$

The Green's function for equation (4.47) can be obtained from the solution to the associated homogeneous form of that equation. This Green's function is readily obtainable from textbooks (Ozisik 1980) or (Carslaw and Jaeger 1967):

$$G = \frac{e^{\gamma^2 \tau}}{8\pi r' \sqrt{\pi(t-\tau)}} \left[e^{\frac{-(r-r')^2}{4(t-\tau)}} - e^{\frac{-(r+r')^2}{4(t-\tau)}} \right] \tag{4.48}$$

Then, going back in the transformation, the free space Green's function *U* is obtained:

$$U = \frac{G}{r} e^{-\gamma^2 t} = \frac{e^{-\gamma^2 (t-\tau)}}{8\pi r r' \sqrt{\pi (t-\tau)}} \left[e^{\frac{-(r-r')^2}{4(t-\tau)}} - e^{\frac{-(r+r')^2}{4(t-\tau)}} \right] \tag{4.49}$$

For being able to use this fundamental solution in the Green's function solution equation, (4.49) must be multiplied by the factor 4π. The reason for doing this has to do with the formulation adopted here for expressing the temperature in terms of the Green's function, *i.e.* the Green's function solution equation presented in section 4.2.3 below.

$$\boxed{U_{(r,t|r',\tau)} = \frac{H_{(t-\tau)} e^{-\gamma^2 (t-\tau)}}{2 r r' \sqrt{\pi (t-\tau)}} \left[e^{\frac{-(r-r')^2}{4(t-\tau)}} - e^{\frac{-(r+r')^2}{4(t-\tau)}} \right]} \tag{4.50}$$

4.2.3 Green's Function Solution Equation

The general solution for the temperature profile in infinite domains, obtained from the bio-heat equation taking into account the blood perfusion, is given in terms of the free-space Green's function in dimensionless form as:

$$\Theta_{(x,t)} = \int x'^{p} U_{(x,t|x',\tau)_{|\tau=0}} F_{(x')} dx' + \int_{\tau=0}^{t} \int x'^{p} U_{(x,t|x',\tau)} H_{(x',\tau)} dx' d\tau \tag{4.51}$$

Where x'^{p} is the Sturm-Liouville weigth function: $p = \begin{cases} 0 \rightarrow \text{infinite slab} \\ 1 \rightarrow \text{infinite cylinder} \\ 2 \rightarrow \text{infinite sphere} \end{cases}$

$U_{(x,t|x',\tau)}$ represents the temperature distribution in an infinite medium at the location ***x***, at time *t*, due to an instantaneous point source of unit strength, located at the point ***x'***, releasing its heat spontaneously at time $t = \tau$.

$U_{(x,t|x',\tau)_{|\tau=0}}$ in equation (4.51) is the free-space Green's function evaluated at $\tau = 0$; $F_{(x')}$ represents the initial condition; and $H_{(x',\tau)}$ includes all the sinks and/or sources.

4.2.4 Finite Fourier Transform

This is an analytical method that consists in expanding the solution of a linear partial differential equation in terms of a set of known functions, called basis functions. After which the problem is reduced to one of finding the spectral coefficients of the expansion:

$$\Theta_{(x,t)} = \sum_{n=1}^{\infty} \Phi_{n(x)} \Theta_{n(t)} \tag{4.52}$$

Where $\Theta_{(x,t)}$ is the unknown temperature; $\Phi_{n(x)}$ are the basis functions; and $\Theta_{n(t)}$ are the spectral coefficients.

The method is applicable to linear problems where at least one coordinate is finite and one attractive feature is that it is more flexible and more direct than separation of variables where as many sub-problems as non-homogeneities present in the original problem must be solved in order to get the final solution by superposition of the solutions of the sub-problems.

The sets of functions suitable to be used as basis functions are the solutions of certain type of eigenvalue problems, called eigenfunctions:

$$L_x \Phi_{(x)} = -\lambda^2 \Phi_{(x)} \tag{4.53}$$

Where L_x is a linear differential operator; $\Phi_{(x)}$ are the eigenfunctions; and λ are the eigenvalues. For an expansion like (4.52) to be valid, the set of basis functions $\Phi_{n(x)}$ must be orthogonal. It can be proved that a sufficient condition for the basis functions to form an orthogonal set, is the differential operator L_x to be self-adjoint. Any Sturm-Liouville

eigenvalue problem meet these conditions, *i.e*, the differential operator is self-adjoint and, then, the eigenfunctions are orthogonal with respect to a weighting function usually called $w_{(x)}$ in literature. The boundary conditions for an eigenvalue problem must be any combination of the homogeneous version of the Dirichlet, Neumann, and Robin types. The operator L_x may be recognized by inspection of the conservation equation by selecting those terms containing *x*.

Once the differential operator is identified and the appropriate basis functions selected, the next step is transform the differential equation along with the initial and boundary conditions with respect to the basis function and the weighting function in the interval of orthogonality as many times as needed to end up with an ordinary differential equation. Then this equation is solved in the transformed domain to get the solution for the spectral coefficients $\Theta_{n(t)}$. The transformation is defined as:

$$\Theta_{n(t)} = \int_0^L w_{(x)} \Phi_{n(x)} \Theta_{(x,t)} dx \tag{4.54}$$

Where $\Theta_{(x,t)}$ is the dependent variable and $w_{(x)}$ is the Sturm-Liouville weighting function.

Besides of being orthogonal, the basis functions are required to be normalized in the interval because in this way $\Theta_{n(t)}$ is the spectral coefficient itself. Otherwise, the spectral coefficient of the expansion would differ with $\Theta_{n(t)}$ by a constant, the norm. Using the inner product notation the orthonormal condition is expressed as:

$$\int_0^L w_{(x)} \Phi_{n(x)} \Phi_{m(x)} dx = \left\langle \Phi_{n(x)}, \Phi_{m(x)} \right\rangle = \delta_{nm} \tag{4.55}$$

Where $0 \le x \le L$ is the interval of orthonormality; and δ_{nm} is the Kronecker delta.

Because for the Sturm-Liouville problem to exist a finite dimension is needed, the transformation is always performed over the finite coordinates. For instance, in a one-dimensional transient heat diffusion problem in a finite region, the transformation would be carried out over the spatial coordinate (time domain is semi-infinite).

When the solution for the transformed temperature and the spectral coefficients of the series expansion of the solution $\Theta_{n(t)}$ is obtained, substitution in equation (4.52) provides the temperature field. The exact solution results when the summation is carried out over all the eigenvalues, *i.e.* $n = \infty$.

For a detailed theoretical presentation of the method the textbooks of (Deen ; Ozisik 1968) are suggested.

5 RESSULTS AND DISCUSSION

In this chapter, the solutions developed in the previous chapter are plotted and the discussion of the results is addressed. For this aim, typical values of tissue thermal properties are adopted as given by (Deng and Liu 2002; Bagaria and Johnson 2005): $\rho_t = \rho_b = 1{,}000$ kg/m^3; $c_t = c_b = 3{,}800$ J/kg°C; $T_a = 37$ °C; $k = 0.5$ W/m°C; $q_{met} = 700$ W/m^3; $\omega_b = 0.0005$ (ml/s)/ml (volumetric blood flow, per ml of tissue).

In order to establish an order of magnitude in the heat generation rate of the particles, a concentration of 10×10^{-3} g of magnetite per gram of tissue, which is a normal dosage reported in clinical trials (C.F. Chan, B. Kirpotin et al. 1993), is assumed. Setting the magnetic field intensity in 6.5 kAm^{-1} and the frequency at 500 kHz (values in between the safety threshold), substitution in the model depicted in Section 2.5 yields a linear relationship between the power P and the volume fraction of particles, ϕ.

The ferrofluid is assumed to be a colloidal suspension of monodisperse magnetite single-domain particles of 12 nm diameter. Correspondingly all the properties required in the expression of the power loss are that of the magnetite (Rosensweig 2002).

So, for magnetite water based ferrofluid under a magnetic field of the features depicted above, equation (2.11) is reduced to:

$$P = 2.495\times10^{8}\,\phi\left[W/m^3\right] \tag{5.1}$$

10×10^{-3} g of magnetite per gram of tissue is equivalent to $\phi \approx 0.003$ establishing a power of:

$$P = 748500\left[W/m^3\right] \tag{5.2}$$

This value will be regarded as the maximum value feasible for the simulations. However, higher losses can be achievable by using ferrofluids with higher SAR values or higher

magnetic field intensity. Recall that the upper limit is 15 kAm^{-1} (Atkinson, Brezovich et al. 1984).

5.1 Numerical Solutions

5.1.1 Monte Carlo Solutions

The geometry being considered for obtaining the Monte Carlo solution was a cube of side length L=0.2 m. In order to solve the temperature for an sphere of radius R=0.1m, the random walkers were instructed to tally the boundary condition when they reach the surface of the sphere. The grid constructed for the walkers to wander through had 27 nodes in each direction. This is a coarse grid but it is enough to get an approximated profile. Beside this fact, as a comparison, the time required for calculations with 40 nodes in each direction is more than 2 hours in a computer with a core 2 duo processor running at 2.26 GHz while the time required for 27 nodes is reduced to 20 minutes. This computational time is not a linear function of the grid size because an increase in the number of grid points translates in more steps for the random walker to take until a boundary or an initial time is reached. But because of the random motion of the walker, the number of steps does not necessarily follow a linear trend.

The boundary condition is:

$$T_{(r=R,t)} = T_a \tag{5.3}$$

Where R is the radius of the sphere.

The nanoparticles are modeled as point sources whose generalized form is:

$$\dot{Q}_{gen(x,y,z,t)} = P_{(x_0,y_0,z_0,t)}\delta_{(x-x_0)}\delta_{(y-y_0)}\delta_{(z-z_0)} \tag{5.4}$$

Where P is the point heating power in W, δ is the Delta of Dirac function, and (x_0,y_0,z_0) is the position of the point-heating source. The strength for each point source is P=0.3 W.

A slice of the domain corresponding to the plane y=0.1m is shown in Figure 5.1 where the size of the sample was N=5000 and N=2000 Random Walks for the plot in the left and the one in the right side, respectively. Next, in Figure 5.2, the profile for N=1200 is shown. As can be seen, with 5000 Random Walks the temperatures field is smooth enough to consider sufficient trials for the computation of temperatures. All these figures show the results of the simulations differing only in the number of random walkers dispatched.

The time consumption for the calculation of the temperature field is higher than that required by, for instance, the finite volume method but, as it was mentioned in the introduction, getting an approximation of the temperature for a point is very fast, even though for sample sizes as large as N=10000.

Following with the analyses of the results, Figure 5.1 must be compared with Figure 5.3 that shows the temperature profile obtained by means of the Finite Volumes Method. Further in the next section, an analytical solution is compared with the Finite Volumes solution in Figure 5.5 in order to validate the codes.

The profiles exhibit a fast decay in temperature as one move away from the sources. The effects of heat removal due to blood perfusion along with a low thermal conductivity and the highly localized heat deposition are the principal responsible factors of this behavior. A better visualization is provided by the figures showing the analytical results that are discussed further in this chapter.

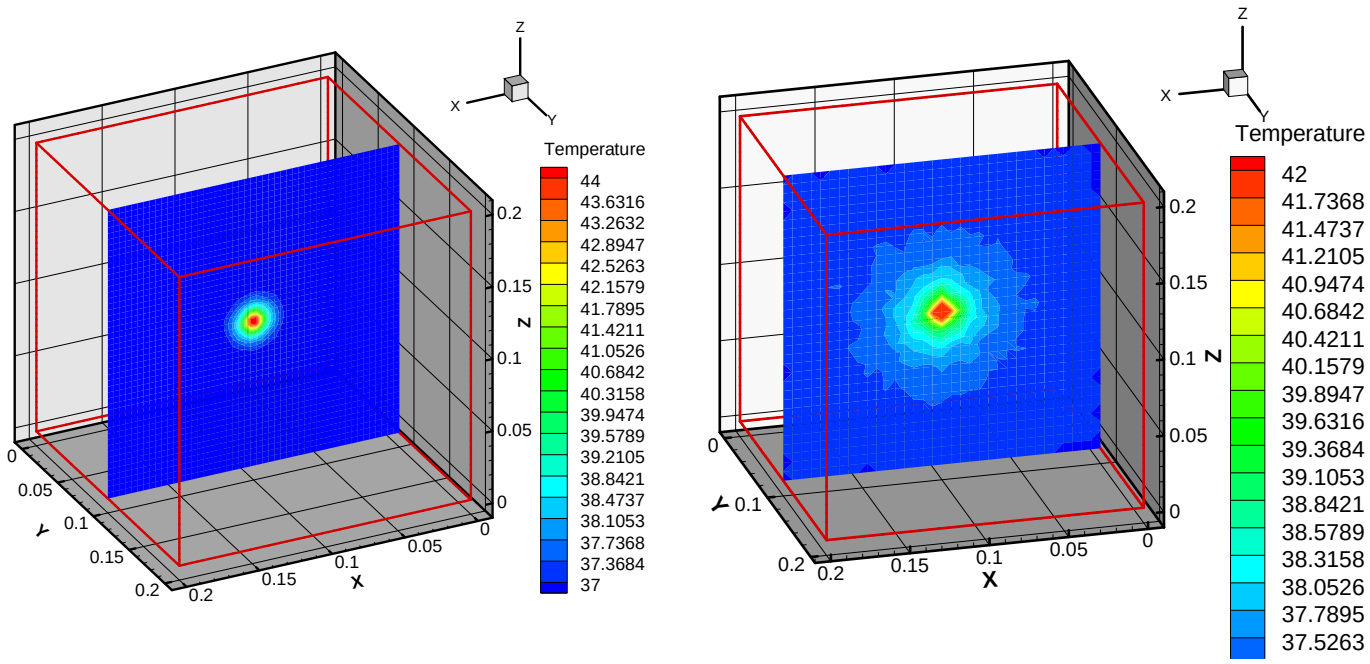

Figure 5.1: Approximated Temperature Profile. Left: N=5000; Right: N=2000

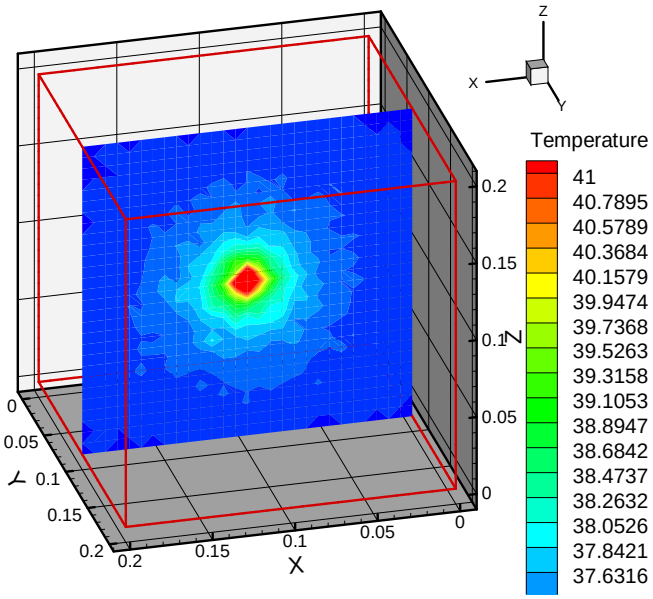

Figure 5.2: Approximated Temperature Profile. N=1200

5.1.2 Finite Volumes Solutions

The values for the thermo-physical are the same of the previous section. Figure 5.3 shows the slice at *y*= 0.1m of the cubic domain of tissue. In order to work with a Cartesian grid, the thermal conductivity inside the cube takes two different values according the control volume face is within a sphere of 0.1 m of diameter or not. A very large value was set for those control volumes outside the sphere and 0.5 W/(mK) for the ones inside the region. This is an easy way to model a sphere using a Cartesian grid, avoiding to work with irregular shaped control volumes. The result is like shrinking the boundaries to the sphere's surface making the problem equal to the one depicted in the previous section.

A 37 °C isothermal surface is shown in Figure 5.4 where it is visible the shrinking of the boundaries to the surface of the sphere.

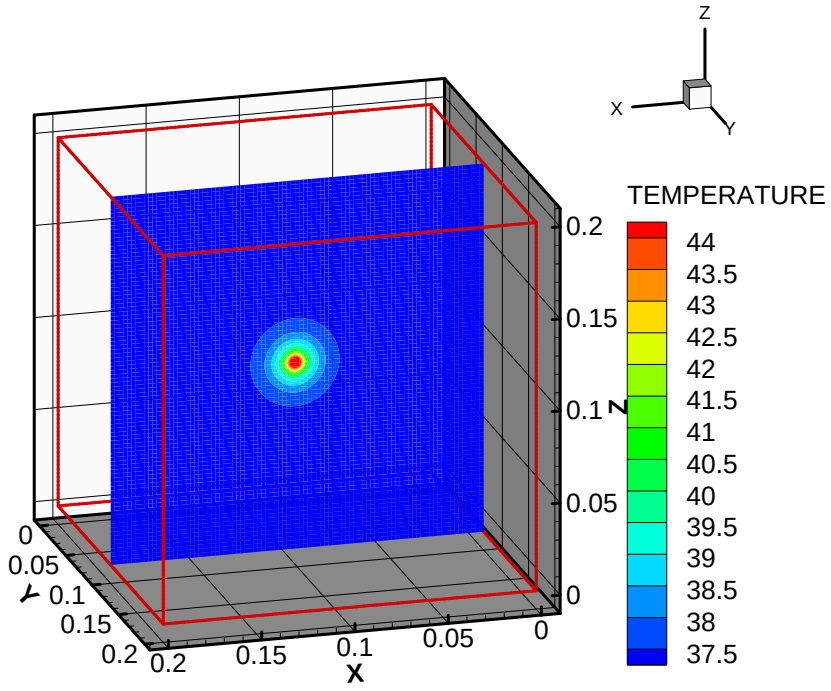

Figure 5.3: Steady Finite volume Solution for a Generating Spherical Subdomain

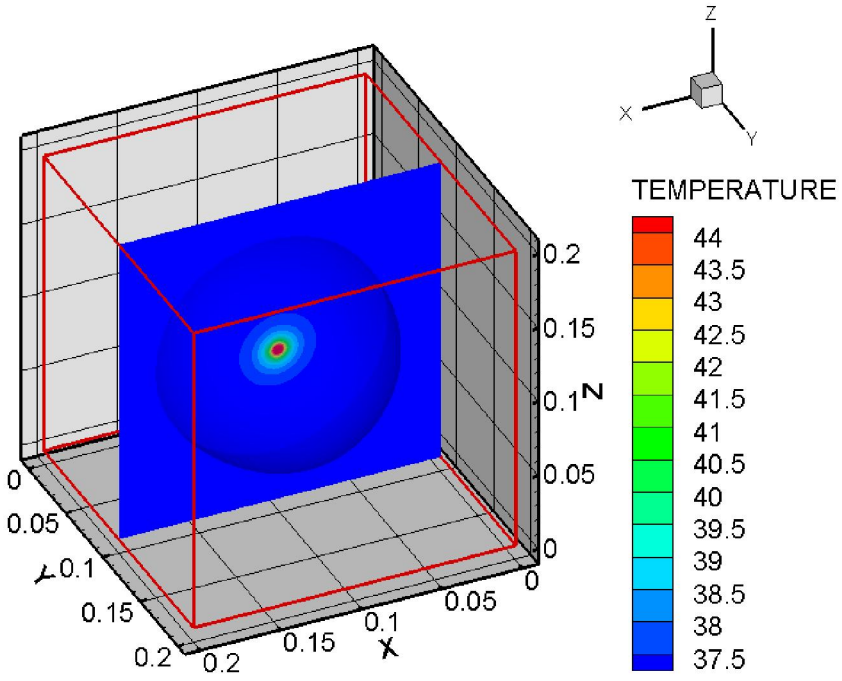

Figure 5.4: 37 C Isothermal surface

For validating the numerical code, a comparison for the steady state temperature distribution is shown in Figure 5.5. Here, q_{met} = 0.0 W/m^3, the spherical source has a radius of r_0= 0.005m and a power of Q_{gen}= 572,958.0 W/m^3, the radius of the domain is R= 0.1 m.

As it can be seen there is a good agreement between both solutions. The difference is due to the coarse grid used. It is not worthy to make a refinement of the grid because the solution is shown to be close enough to the analytical one.

In Figure 5.6 is shown that grid independence of the solution is reached for N=110. This number means that the grid consists in 110 nodes in each direction of the cube. Thus, the number of nodes and, therefore, unknowns is 110^3=1,331,000. Recall that in the finite volume method, as well as the Monte Carlo method, the temperature in the grid points is evaluated.

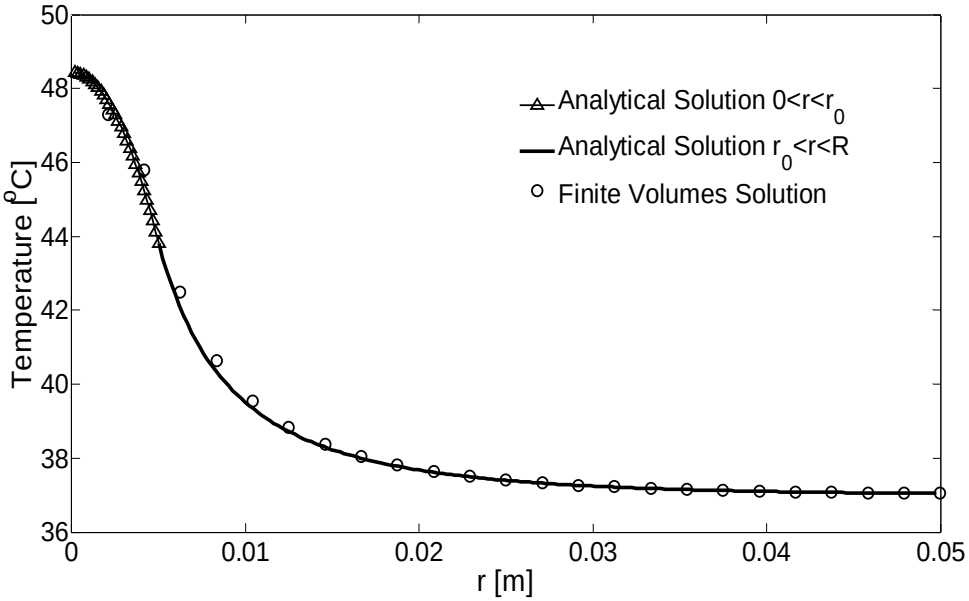

Figure 5.5: Steady Analytical vs Finite Volume Solution. Radius of the Spherical Source: r_0=0.005 m. q_{met}=0; Q_{gen}= 572,958 W/m^3

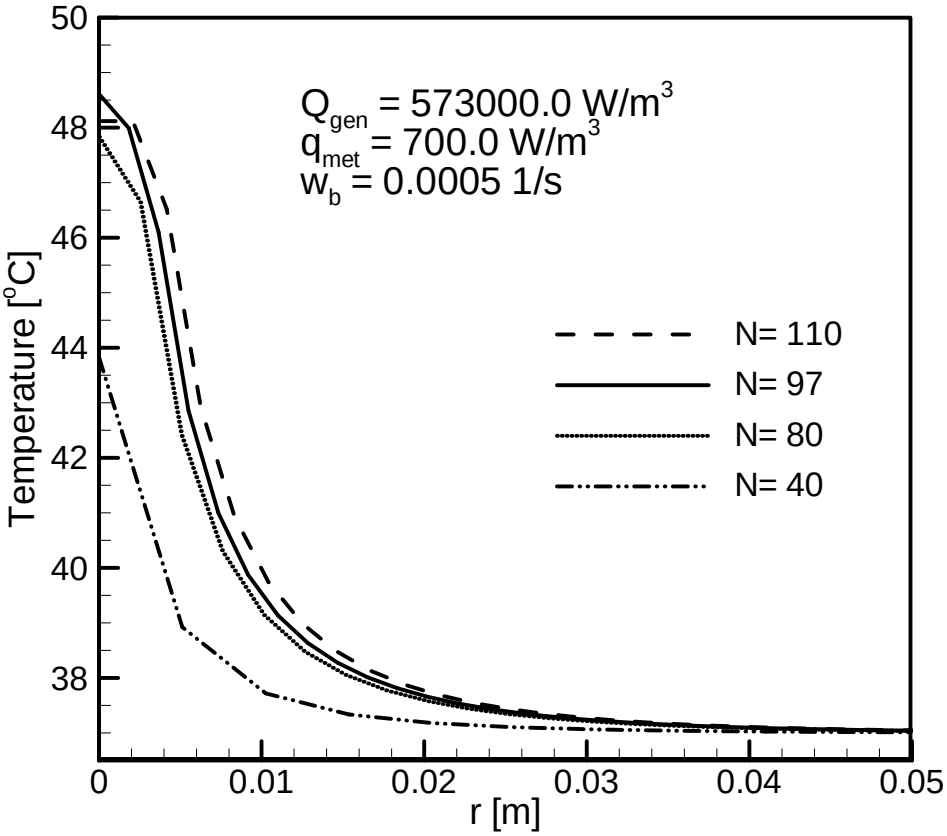

Figure 5.6: Grid Independence in the Solution. N is the number of nodes in each direction.

5.2 Analytical Solutions

In the following subsections the analytical solutions are developed by the methods exposed in Chapter 4. Each transient solution is plotted for several time steps with the highest time level corresponding to the steady state condition.

5.2.1 Plane Source Solution in an Infinite Domain

The equation that models the problem is the 1-D version of equation (3.7) in Cartesian coordinates:

$$\frac{\partial \Theta_{(x,t)}}{\partial t} = \frac{\partial^2 \Theta_{(x,t)}}{\partial x^2} + \gamma^2 \Theta_{(x,t)} + H_{(x,t)} \tag{5.5}$$

$t > 0$; $-\infty < x < \infty$

$$\Theta_{(x,0)} = 0 \tag{5.6}$$

Where $H_{(x,t)} = q + Q_{(x,t)}$ is the generalized source term. Note that all the variables are dimensionless. Because there is no characteristic length, the spatial variable x is dimensionalized with respect to unity.

Using the principal solution (4.34) and replacing it in the general solution equation (4.51), the solution for the bio-heat equation in infinite domains in Cartesian coordinates is obtained by setting the exponent p to be zero:

$$\Theta_{(x,t)} = \int_{\tau=0}^{t} \int_{x'=-\infty}^{\infty} U_{(x,t|x',\tau)} H_{(x',\tau)} dx' d\tau \tag{5.7}$$

Splitting the source H in two parts, one corresponding to the metabolic heat generation and another one modeling a plane source, the solution (5.7) reads like

$$\Theta_{(x,t)} = \int_{\tau=0}^{t} \int_{x'=-\infty}^{\infty} \frac{1}{\sqrt{4\pi(t-\tau)}} e^{-\frac{(x-x')^2}{4(t-\tau)} - \gamma^2(t-\tau)} \left(q + Q_{(x',\tau)}\right) dx' d\tau \tag{5.8}$$

Now $Q_{(x',\tau)}$ represents a plane source releasing its heat at x=0 continuously form t=0. Its mathematical representation is given by $Q_{(x',\tau)} = P_{s_{(\tau)}} \delta_{(x')}$ where $P_{s_{(\tau)}} = \frac{g_{s_{(\tau)}}}{kT_a}$ is the dimensionless source strength; $g_{s_{(\tau)}}$ (W/m^2) is the strength of the source and it may be time dependent. Substituting this expression in equation (5.8) the temperature distribution is:

$$\Theta_{(x,t)} = \int_{\tau=0}^{t} \frac{1}{\sqrt{4\pi(t-\tau)}} \int_{x'=-\infty}^{\infty} q e^{-\frac{(x-x')^2}{4(t-\tau)} - \gamma^2(t-\tau)} dx' d\tau + \int_{\tau=0}^{t} \frac{P_{S(\tau)}}{\sqrt{4\pi(t-\tau)}} e^{-\frac{x^2}{4(t-\tau)} - \gamma^2(t-\tau)} d\tau \tag{5.9}$$

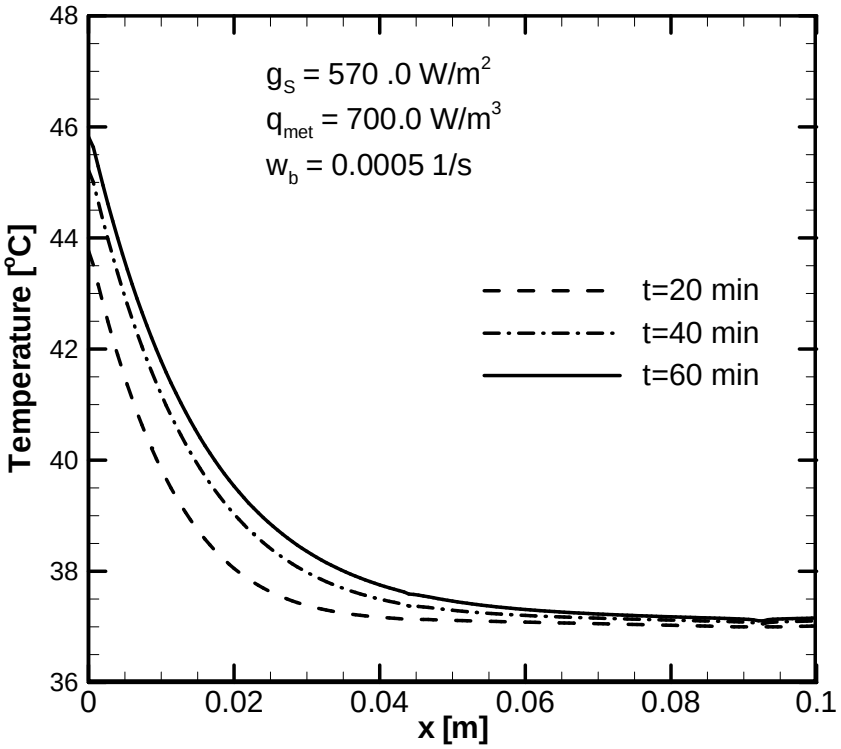

Figure 5.7: Transient Temperature Distribution due to a Plane source in an Infinite Domain

With the normal value of volume fraction concentration of $\phi \approx 0.003$ and the generation rate predicted by the heat generation model of Rosensweig, it was shown at the beginning of this chapter that a heat deposition of 748500 (W/m^3) is achievable with magnetite particles.

In order to reach therapeutic temperatures, having the particles disposed in a planar region of tissue, a thickness of 0.76 mm is needed which means a generation rate of 570 W/m^2. The transient temperature profiles for this particular configuration of the magnetic nanoparticles are shown in Figure 5.7.

5.2.2 Line Source Solution in an Infinite Domain

The mathematical formulation is given by:

$$\frac{\partial \Theta_{(r,t)}}{\partial t} = \frac{1}{r}\frac{\partial}{\partial r}\left(r \frac{\partial \Theta_{(r,t)}}{\partial r} \right) + \gamma^2 \Theta_{(r,t)} + H_{(r,t)} \tag{5.10}$$

$t > 0 \; ; \; 0 \le r < \infty$

$$\Theta_{(0,t)} = \text{ finite} \tag{5.11}$$

$$\Theta_{(r,0)} = 0 \tag{5.12}$$

Using the free-space Green's function obtained for this case, equation (4.45), in the general solution (4.51) and letting the exponent *p* of the spatial variable to be unity, the solution is written as follows:

$$\Theta_{(r,t)} = \int_{\tau=0}^{t} \int_{r'=0}^{\infty} r' U_{(r,t|r',\tau)} H_{(r',\tau)} dr' d\tau \tag{5.13}$$

Then, recalling that $H_{(r',\tau)} = q + Q_{(r',\tau)}$:

$$\Theta_{(r,t)} = \int_{\tau=0}^{t} \int_{r'=0}^{\infty} \frac{1}{2(t-\tau)} I_0\left(\frac{rr'}{2(t-\tau)}\right) e^{-\frac{\left(r^2+r'^2\right)}{4(t-\tau)} - \gamma^2 (t-\tau)} \left(q + Q_{(r',\tau)} \right) dr' d\tau \tag{5.14}$$

Now, the relationship between the volumetric source $Q_{(r',\tau)}$ and a line source releasing its heat at $r=0$ continuously from $t=0$ is $Q_{(r',\tau)}=\frac{P_{L_{(\tau)}}}{2\pi r'}\delta_{(r')}$, where $P_{L(\tau)}=\frac{g_{L(\tau)}}{kT_a}$ is the dimensionless strength of the line source and may be time-dependent. $g_{L(\tau)}$(W/m) is the dimensional strength of the source. The substitution of this expression for $Q_{gen(r',\tau)}$ in (5.14) and performing the integral, the expression for the temperature distribution is:

$$\Theta_{(r,t)}=\int_{\tau=0}^{t}\int_{r'=0}^{\infty} qr'\frac{I_0\left(\frac{rr'}{2(t-\tau)}\right)}{2(t-\tau)}e^{-\frac{\left(r^2+r'^2\right)}{4(t-\tau)}-\gamma^2(t-\tau)}dr'd\tau+\int_{\tau=0}^{t}\frac{P_{L(\tau)}}{4\pi(t-\tau)}e^{-\frac{r^2}{4(t-\tau)}-\gamma^2(t-\tau)}d\tau \qquad (5.15)$$

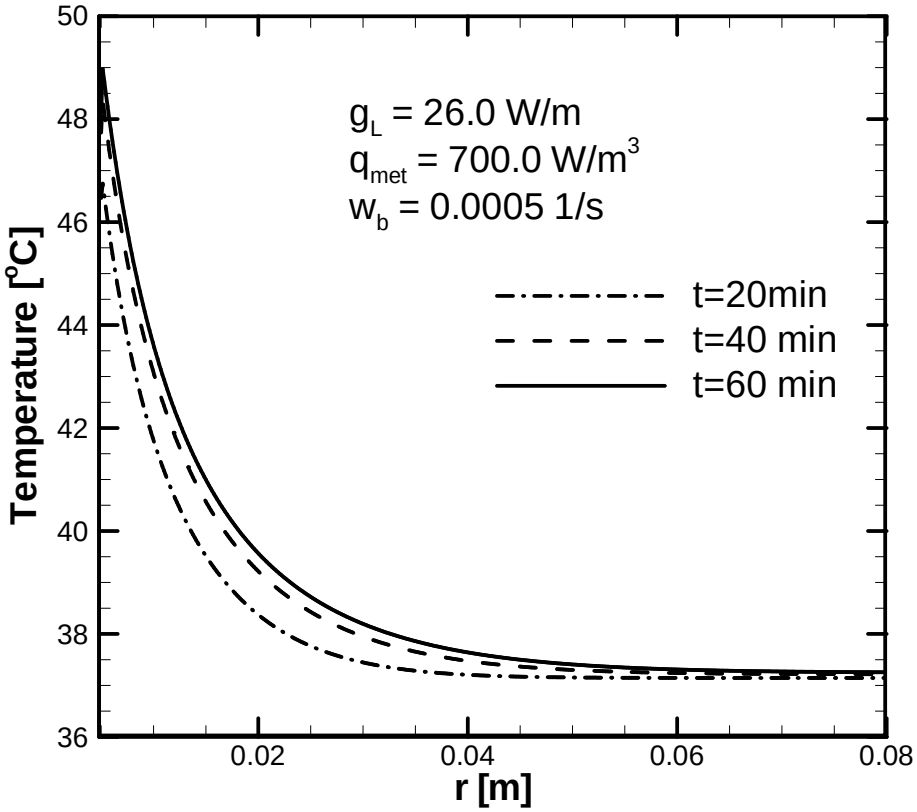

Figure 5.8: Transient Temperature Distribution due to a Line source in an Infinite Domain

In order to achieve therapeutic temperatures with a generation of P=784500 (W/m^3), the radius of the line source must be $r = \sqrt{\frac{g_L}{\pi P}} = 3.33$ mm. The transient temperature profiles yielded by this particular configuration of the sources are shown in Figure 5.8.

5.2.3 Point Source Solutions

5.2.3.1Finite Spherical Domain

The mathematical formulation for a spherical domain with an arbitrary source term is (from equation (3.7)):

$$\frac{\partial \Theta_{(r,t)}}{\partial t} = \frac{1}{r^2}\frac{\partial}{\partial r}\left(r^2 \frac{\partial \Theta_{(r,t)}}{\partial r} \right) - \gamma^2 \Theta_{(r,t)} + H_{(r,t)} \tag{5.16}$$

$t > 0 \; ; \; 0 \le r < 1$

$$\Theta_{(0,t)} = \text{finite} \tag{5.17}$$

$$\Theta_{(1,t)} = 0 \tag{5.18}$$

$$\Theta_{(r,0)} = 0 \tag{5.19}$$

Where $H_{(r,t)} = q + Q_{(r,t)}$.

Defining a new variable $\Phi_{(r,t)} = re^{\gamma^2 t}\Theta_{(r,t)}$, and substituting:

$$\frac{\partial \Phi_{(r,t)}}{\partial t} = \frac{\partial^2 \Phi_{(r,t)}}{\partial r^2} + H_{(r,t)} re^{\gamma^2 t} \tag{5.20}$$

$t \ge 0 \; ; \; 0 \le r \le 1$

$$\Phi_{(0,t)} = 0 \tag{5.21}$$

$$\Phi_{(1,t)} = 0 \tag{5.22}$$

$$\Phi_{(r,0)} = 0 \tag{5.23}$$

By using the Finite Fourier Transform method, the solution is given by:

$$\Phi_{(r,t)} = \sum_{n=1}^{\infty} \Phi_{n(t)} \phi_{n(r)} \tag{5.24}$$

Where $\phi_{n(r)} = \sqrt{2}\sin(\lambda_n r)$ are the basis function; $\lambda_n = n\pi$; $n = 1,2,3,...$ are the eigenvalues of the associated Sturm-Liuville problem; and $\Phi_{n(t)}$ are the spectral coefficients of the Fourier expansion (5.24).

In order to obtain an expression for the spectral coefficients, the partial differential equation (5.20) is transformed with respect to the basis functions $\phi_{n(r)}$ and the weighting function (which is unity for equation (5.20) accordingly to the associated Sturm-Liuville problem). The transformation of each term of equation (5.20) yields:

$$\int_0^1 \frac{\partial \Phi}{\partial t} \phi_n dr = \frac{d\Phi_n}{dt} \tag{5.25}$$

$$\int_0^1 \frac{\partial^2 \Phi}{\partial r^2} \phi_n dr = -\lambda_n^2 \Phi_n \tag{5.26}$$

$$\int_0^1 qre^{\gamma^2 t} \phi_n dr = -\sqrt{2}\frac{(-1)^n}{\lambda_n} qe^{\gamma^2 t} \tag{5.27}$$

$$\int_0^1 Qre^{\gamma^2 t} \phi_n dr = -\sqrt{2}\frac{P\lambda_n}{4\pi} e^{\gamma^2 t} \tag{5.28}$$

In equation (5.28), $Q = \frac{P^* \delta_{(r)}}{4\pi r^2}$, which is the mathematical representation of a point source located at *r*=0. The * means that *P* is in the dimensionless space.

Subtitution of equations (5.25)-(5.28) in equation (5.20) yields:

$$\frac{d\Phi_n}{dt} + \lambda_n^2 \Phi_n = A_n e^{\gamma^2 t} \tag{5.29}$$

The transformed initial condition (5.23) is:

$$\Phi_{n(0)} = 0 \tag{5.30}$$

Where $A_n = \sqrt{2}\left[\frac{P^*\lambda_n}{4\pi} - \frac{q}{\lambda_n}(-1)^n\right]$.

The solution of the ordinary differential equation of order one, (5.29), gives the spectral coefficients $\Phi_{n(t)}$:

$$\Phi_{n(t)} = \frac{A_n}{\left[\lambda_n{}^2 + \gamma^2\right]}\left[e^{\gamma^2 t} - e^{-\lambda_n{}^2 t}\right] \tag{5.31}$$

Then:

$$\Phi_{(r,t)} = \sum_{n=1}^{\infty}\Phi_{n(t)}\phi_{n(r)} = \sum_{n=1}^{\infty}\frac{\sqrt{2}A_n}{\left[\lambda_n{}^2 + \gamma^2\right]}\sin\left(\lambda_n r\right)\left[e^{\gamma^2 t} - e^{-\lambda_n{}^2 t}\right] \tag{5.32}$$

Finally the temperature is given by $\Theta_{(r,t)} = \frac{\Phi_{(r,t)}}{r}e^{-\gamma^2 t}$:

$$\Theta_{(r,t)} = \frac{2}{r}\sum_{n=1}^{\infty}\left[\frac{P^*\lambda_n}{4\pi} - \frac{q}{\lambda_n}(-1)^n\right]\frac{\sin\left(\lambda_n r\right)}{\left(\lambda_n{}^2 + \gamma^2\right)}\left[1 - e^{-\left(\gamma^2 + \lambda_n{}^2\right)t}\right] \tag{5.33}$$

Figure 5.9 shows the transient response in temperature at different times due to a point source located at the center of a sphere of radius R=0.1 m. The solution has a singularity at r=0 which is represented by the factor 1/r in equation (5.33).

This figure reveals the highly localized effect of a point source. A fast decay in temperature with the radial coordinates is observed which is expected given that the effective thermal conductivity for the tissues is very small. This effect is discussed in detail in Section 5.2.4.

A single iron nanoparticle can generate 1.2×10^9 (W/m^3) (Rabin 2002). Then, the energy released by this single particle, considering it is of 10 nm radius and of spherical shape, is $1.2\times10^9\frac{4}{3}\pi\left(10\times10^{-9}\right)^3 = 5.03\times10^{-15}$ (W). Note from Figure 5.9 that 0.08 (W) are required for a single particle in order to achieve a temperature rise of 12 °C.

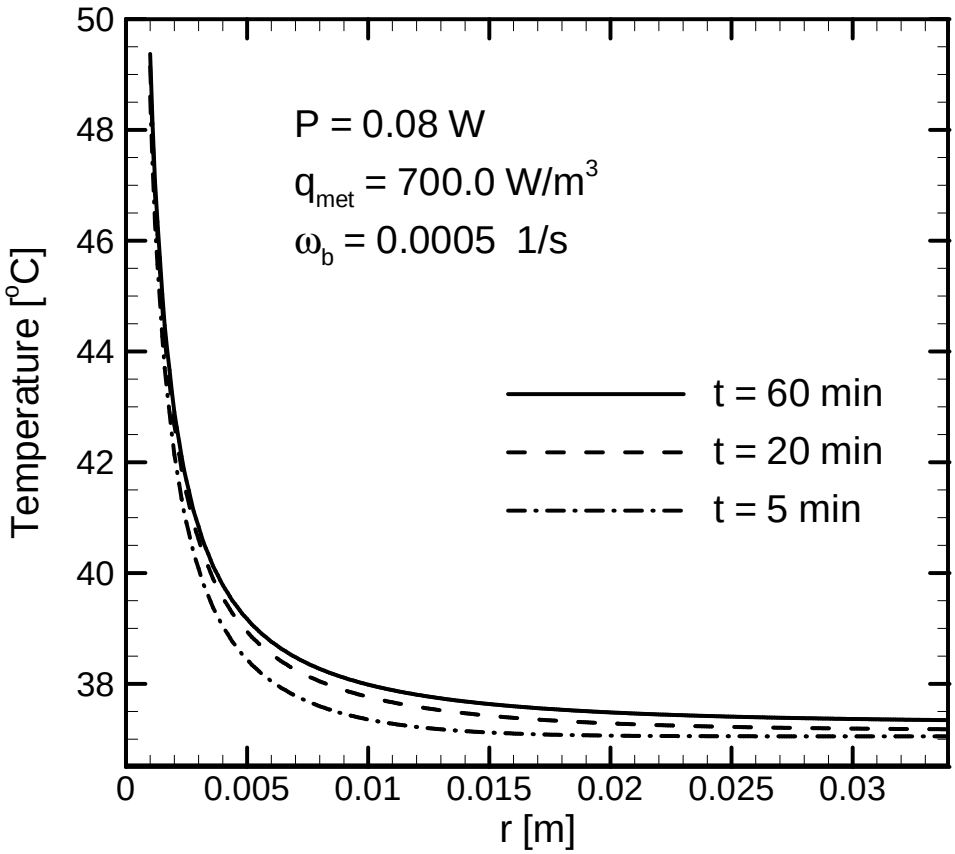

Figure 5.9: Transient Point Source Solution for a Finite Sphere

This analyses highlights that the solely action of one single particle is not enough to reach therapeutic values for the temperatures. Instead, there must be distributed in a certain region within the tumor as shown in section 5.1.

5.2.3.2 Infinite Spherical Domain

The mathematical formulation for the bio-heat equation in an unbounded 1-D domain is derived from equation (3.7) as:

$$\frac{\partial \Theta_{(r,t)}}{\partial t} = \frac{1}{r^2}\frac{\partial}{\partial r}\left(r^2 \frac{\partial \Theta_{(r,t)}}{\partial r} \right) - \gamma^2 \Theta_{(r,t)} + H_{(r,t)} \qquad (5.34)$$

$t > 0 \; ; \; 0 \le r < \infty$

$$\Theta_{(0,t)} = \text{ finite} \tag{5.35}$$

$$\Theta_{(r,0)} = 0 \tag{5.36}$$

The heat sources allowed by this formulation must be such that axis-symmetrical conditions are present.

Using the Green's function solution equation (4.51), the solution would be:

$$\Theta_{(r,t)} = \int_{\tau=0}^{t} \int_{r'=0}^{\infty} r'^{2} U_{(r,t|r',\tau)} H_{(r',\tau)} dr' d\tau \tag{5.37}$$

Finally, the solution for $\Theta_{(r,t)}$ is expressed as:

$$\Theta_{(r,t)} = \frac{1}{2} \int_{\tau=0}^{t} \int_{r'=0}^{\infty} \frac{r' e^{-\gamma^2 (t-\tau)}}{r\sqrt{\pi (t-\tau)}} \left[e^{\frac{-(r-r')^2}{4(t-\tau)}} - e^{\frac{-(r+r')^2}{4(t-\tau)}} \right] \left(q + Q_{(r',\tau)} \right) dr' d\tau \tag{5.38}$$

Now, $Q_{(r',\tau)}$ represents a point source of strength $P_{P(\tau)}$ releasing its energy at $r = 0$ continuously from times $t = 0$ whose mathematical representation is:

$$Q_{(r',\tau)} = \frac{P_{P(\tau)}}{4\pi r'^{2}} \delta_{(r')} \tag{5.39}$$

Where $P_{P(\tau)} = \frac{g_{P(\tau)}}{kT_a}$ is the dimensionless strength of the source and, correspondingly, $g_{P(\tau)}$ (W) is the dimensional analog.

The integral $\int_{r'=0}^{\infty} r'^{2} UQ dr'$ can be integrated analytically for the source given by (5.39):

$$\frac{1}{8} \int_{\tau=0}^{t} \int_{r'=0}^{\infty} \frac{P_{P(\tau)} \delta_{(r')}}{\pi r'} \frac{e^{-\gamma^2 (t-\tau)}}{r\sqrt{\pi (t-\tau)}} \left[e^{\frac{-(r-r')^2}{4(t-\tau)}} - e^{\frac{-(r+r')^2}{4(t-\tau)}} \right] dr' d\tau = \int_{\tau=0}^{t} \frac{P_{P(\tau)} e^{\frac{-r^2}{4(t-\tau)} - \gamma^2 (t-\tau)}}{8\pi\sqrt{\pi (t-\tau)^3}} d\tau \tag{5.40}$$

Then, the final solution for the point source is:

$$\Theta_{(r,t)} = \frac{1}{r}\int_{\tau=0}^{t}\int_{r'=0}^{\infty}\frac{e^{-\gamma^2(t-\tau)}r'q}{2\sqrt{\pi(t-\tau)}}\left[e^{\frac{-(r-r')^2}{4(t-\tau)}} - e^{\frac{-(r+r')^2}{4(t-\tau)}}\right]dr'd\tau + \frac{1}{8\pi}\int_{\tau=0}^{t}\frac{P_{P(\tau)}e^{\frac{-r^2}{4(t-\tau)}-\gamma^2(t-\tau)}}{\sqrt{\pi(t-\tau)^3}}d\tau \qquad (5.41)$$

Figure 5.10 shows the temperature distribution for different times due to a point source located at the center of an infinite sphere. The solution presents a singular behavior at r=0.

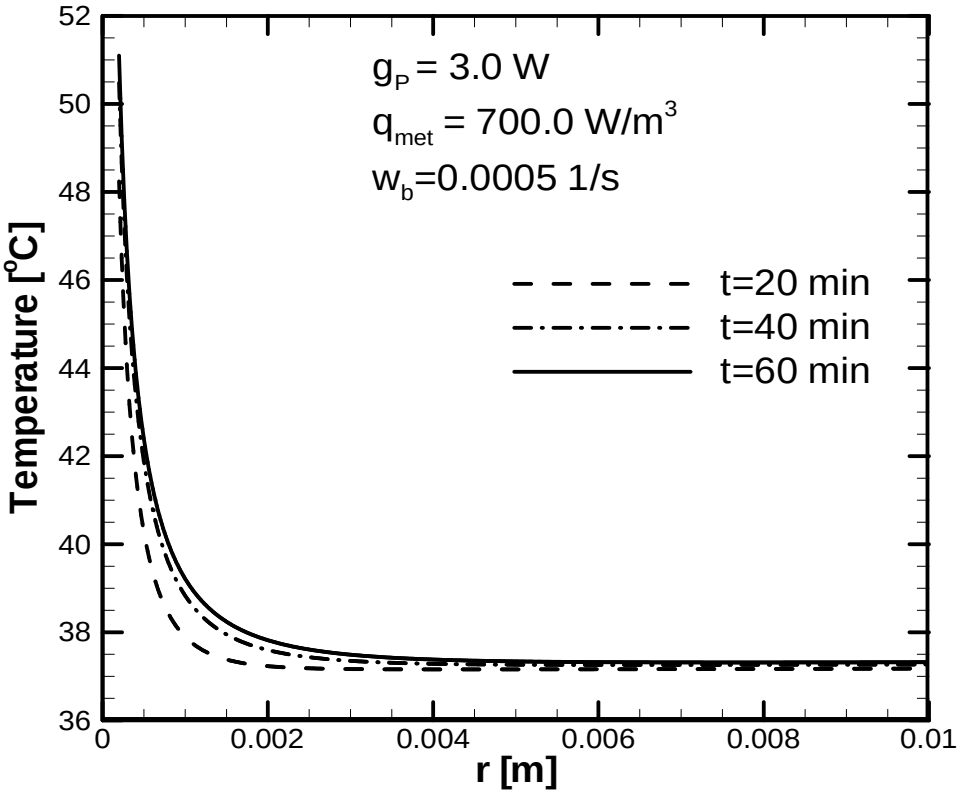

Figure 5.10: Transient Temperature Distribution due to a Point source in an Infinite Domain

Comparing this profile with the one for a finite domain, it can be seen that a higher value for the power of the source is needed in the former to produce the same temperature profile. The explanation of this behavior lies in the fact that the effect of the boundary condition becomes negligible as the domain size goes to infinity.

Observing the profiles produced by the plane, the line and the point sources, it can be seen that, the more localized the source the steeper the change in the temperature profile. Inversely, the temperature penetration depth decreases when the heat deposition is more localized.

5.2.4 Shell Source Solution

The solution for the temperature distribution inside a full sphere is developed here by means of the Finite Fourier Transform. The spherical domain has a shell source at $r = r_0$ being modeled by a Dirac delta function.

Given the symmetry of the problem the temperature is (*r*,*t*) dependent. The mathematical formulation is given by equation (3.7) and it is written down here in a suitable form as:

$$\frac{\partial \Theta}{\partial t} = \frac{1}{r^2}\frac{\partial}{\partial}\left(r^2 \frac{\partial \Theta}{\partial r} \right) - \gamma^2\ \Theta + q + \mathrm{Q}\,; \qquad 0 \le r \le 1,\ t > 0 \tag{5.42}$$

$$\Theta_{(1,t)} = 0 \tag{5.43}$$

$$\Theta_{(r,0)} = 0 \tag{5.44}$$

Performing the transformation $\Theta = \frac{U}{r} e^{-\gamma^2 t}$

$$\frac{\partial U}{\partial t} = \frac{\partial^2 U}{\partial r^2} + (q + Q) r e^{\gamma^2 t} \tag{5.45}$$

$$U_{(0,t)} = 0 \tag{5.46}$$

$$U_{(1,t)} = 0 \tag{5.47}$$

$$U_{(r,0)} = 0 \tag{5.48}$$

The basis function suitable for this problem are

$$\Phi_n = \sqrt{2} \sin(\lambda_n r) \tag{5.49}$$

Where $\lambda_n = n\pi$. The transformation is given by

$$U_{n(t)} = \int_0^1 U_{(r,t)} \Phi_{n(r)} dr \tag{5.50}$$

Taking this transform to each term of the differential equation along with the initial condition:

$$\frac{dU_n}{dt} + \lambda_n^2 U_n = A_n e^{\gamma^2 t} \tag{5.51}$$

$$U_n\big|_{t=0} = 0 \tag{5.52}$$

Where $A_n = \sqrt{2}\left[\frac{P^* \sin(\lambda_n r_0)}{4\pi r_0} - \frac{q(-1)^n}{\lambda_n}\right]$ and Q was replaced by $\frac{P^*}{4\pi r^2}\delta_{(r-r_0)}$ which models the shell source.

The boundary conditions are automatically included when transforming the diffusion term but because of the homogeneity they add nothing to the resulting ordinary differential equation.

The solution of (5.51) and (5.52) is:

$$U_{n(t)} = \frac{A_n}{\left(\lambda_n^2 + \gamma^2\right)}\left[e^{\gamma^2 t} - e^{-\lambda_n^2 t}\right] \tag{5.53}$$
$$\lambda_n = n\pi; \quad n = 1, 2, 3, \ldots$$

Taking the inverse transform, the dimensionless temperature is

$$U_{(r,t)} = \sum_{n=1}^{\infty} \frac{\sqrt{2} A_n}{\left(\lambda_n^2 + \gamma^2\right)} \sin(\lambda_n r)\left[e^{\gamma^2 t} - e^{-\lambda_n^2 t}\right] \tag{5.54}$$

Or, reversing the transformation by $\Theta = \frac{U}{r} e^{-\gamma^2 t}$:

$$\Theta_{(r,t)} = \sum_{n=1}^{\infty} \frac{2}{r\left(\lambda_n^2 + \gamma^2\right)}\left[\frac{P^* \sin(\lambda_n r_o)}{4\pi r_o} - \frac{q(-1)^n}{\lambda_n}\right] \sin(\lambda_n r)\left[1 - e^{-\left(\lambda_n^2 + \gamma^2\right)t}\right] \tag{5.55}$$

Note, from the dimensionless form of the sources, that the relationship between the non-dimensional source and the dimensional one is $P^* = \frac{Pr_0^{*2}}{kT_a r_0^2}$.

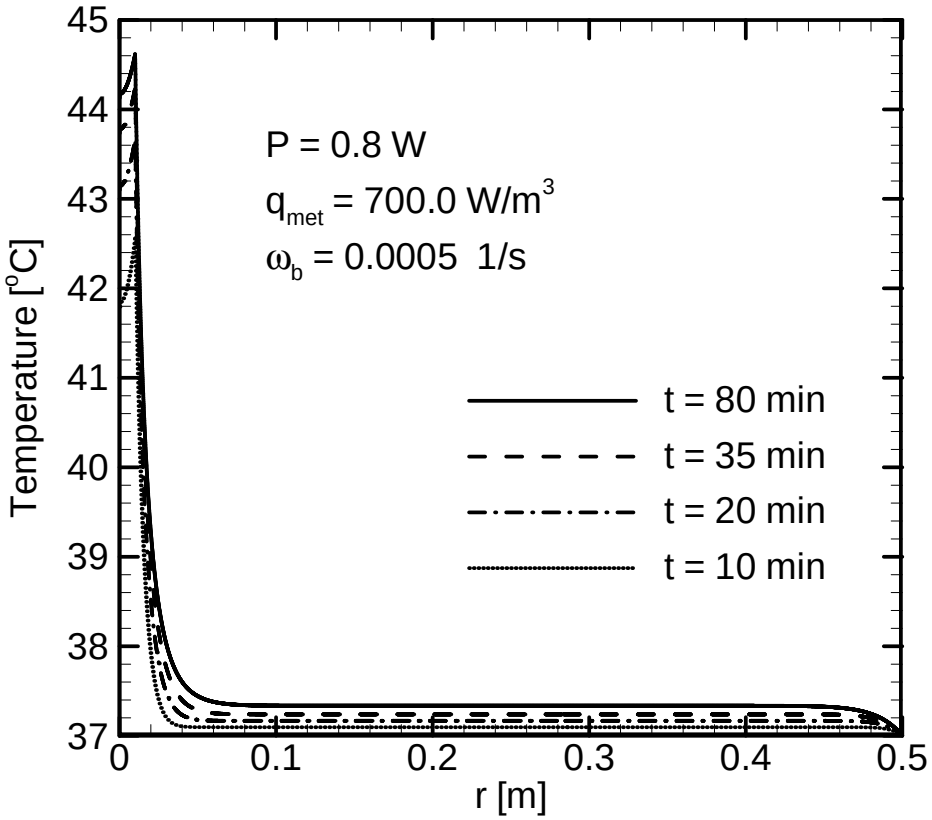

Figure 5.11: Transient Temperature Due to a Shell of Nanoparticles at Tumor Surface. Radius of the shell: r_0=0.01 m.

Valuable information can be extracted from the solution for a shell source. As it can be seen in Figure 5.12, an almost flat temperature profile is obtained inside the region that is modeling the tumor. This is because during the transient the effect of the heat that flows inside this region is to increase the temperature till the steady state value. Once the steady state is reached, temperature gradients are small in this region compared to the gradients present in the outer region corresponding to the healthy tissue. Due to the low thermal conductivity of tissue, according to Fourier's Law, temperature gradients in this zone must be large so the power that is being generated can be diffused producing a steep decrease in

temperature in the healthy tissue. Values for the thermal conductivity of some tissues is presented in Table 5.1 and also it is included the value for water for a comparison.

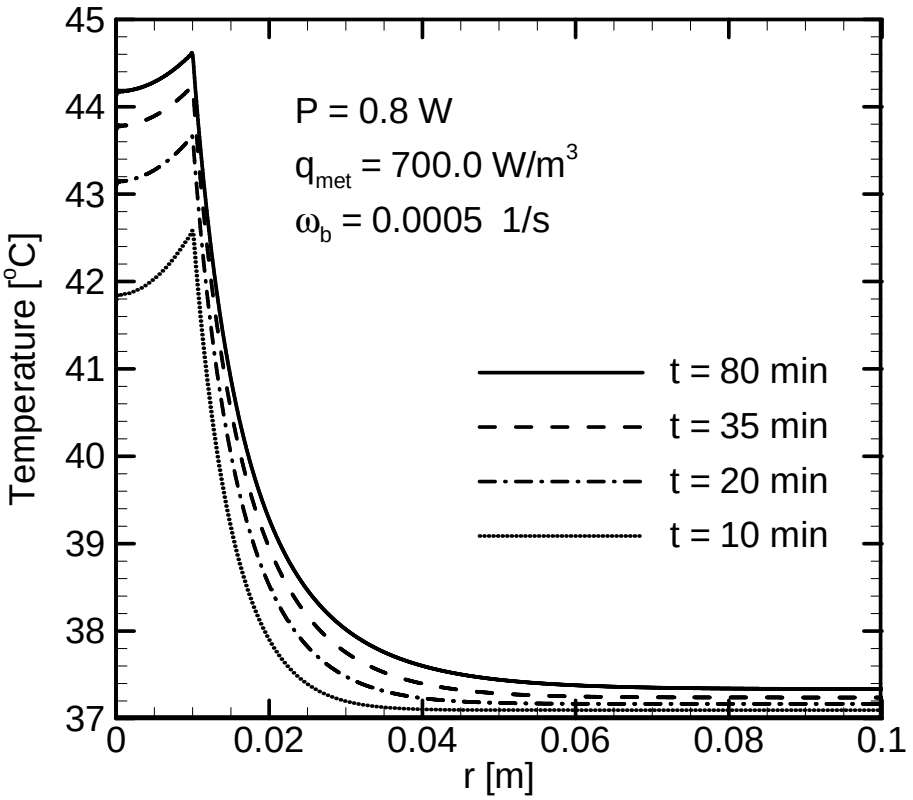

Figure 5.12: Augmented region of Figure 5.11. Radius of the shell: r_0=0.01 m.

This result highlights that a temperature profile close to the ideal therapeutic temperature profile can be achieved if the magnetic nanoparticles are retained by cancerous cells located in the surface of the tumor. This can be done by attaching specific binders to the nanoparticles during the process of synthesis.

Table 5.1: Thermal Conductivity of Some Tissues

Tissue	Thermal Conductivity (*W/m K*)
Tumor periphery	0.511
Tumor core	0.561
Colon cancer	0.545
Bone	0.41-0.63
Blood	$0.492 \pm 9\times10^{-3}$
Pure water	0.627

Considering a spherical solid tumor of 2 cm diameter, the minimum thickness of the shell needed to produce the temperature profile shown in figure Figure 5.12 can be determined. Knowing that 748500 (W/m^3) may be generated, with a volume fraction of particles around 0.03, and that 0.8 (W) are needed to reach therapeutic temperatures, the thickness of the shell can be estimated as:

$$\frac{0.8}{\frac{4}{3}\pi\left(r_2^3 - 0.01^3\right)} = 748500 \tag{5.56}$$

Where r_2 is the outer radius of the generating shell and its value from equation (5.56) is $r_2 = 0.010786$ m yielding a thickness of 7.86×10^{-4} m.

5.2.5 Parametric Analysis

In highly vascularized tumors the blood perfusion rate can be as large as 0.002 ($m^3/s/m^3$) which means that the blood flow could considerably move down the temperature profile and deviate it away from the therapeutic. Besides depending in the vessel network, the perfusion rate is a natural way in which the metabolism regulates the body temperature. Then, it is expected to have higher perfusion rates during the heating.

By plotting the temperature distribution for some values of the perfusion rate within the feasible range the effects over the profile is revealed. For instance, from Figure 5.13 it is clear that the perfusion rate does not modify too much the highest temperature when the heat is deposited highly localized but this is not the case for the penetration depth of the profile. A steep decay in temperature is observed for ω_b= 0.002 s^{-1}.

Figure 5.14 shows the influence of the perfusion rate in the temperature profiles for a shell source which intents to model the nanoparticles deposition in the surface of a tumor.

The negative effect of blood perfusion is that the power to be dissipated within the tumor tissue needs to be higher than the one that would be obtained without blood perfusion, or in other words, for fixed magnetic field conditions (determined by safety and tolerance), the Specific Absorption Rate (SAR) of the ferrofluids must be such that even with the effect of heat removal by perfusion, the therapeutic temperarute is still achievable. On the other hand, blood perfusion helps to reduce the penetration depth in the healthy tissue.

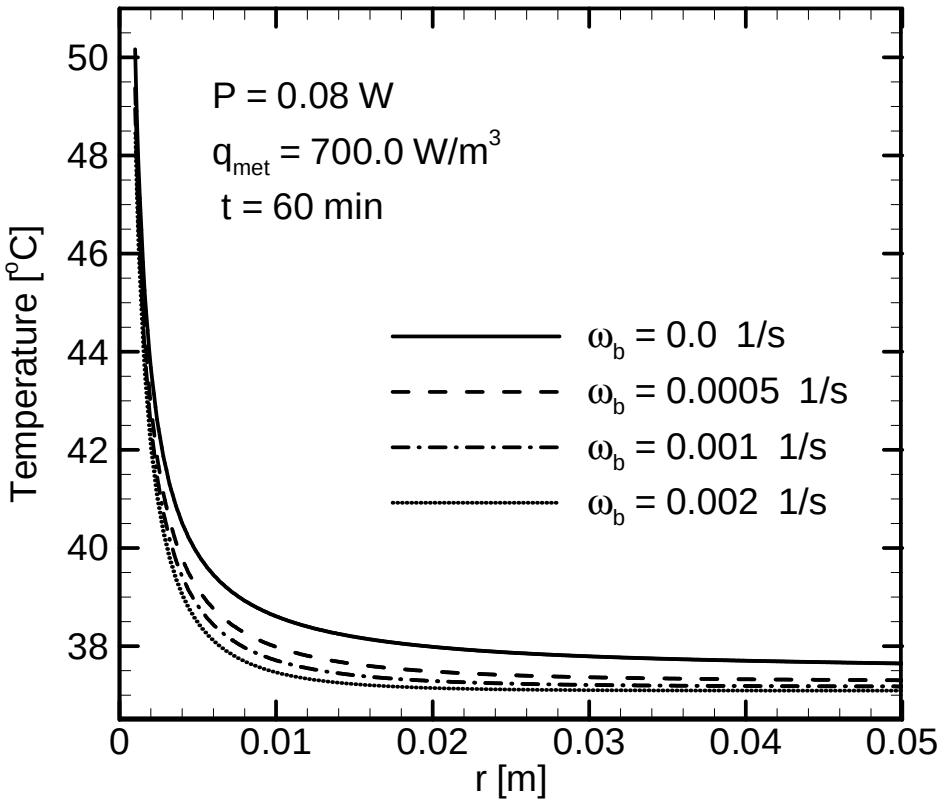

Figure 5.13: Effect of the Blood Perfusion Rate in the Temperature Distribution for a Point Source in a Sphere, *R*=0.1 m

The average time for the temperature to reach the 95% of its steady state value is around forty five minutes and all the plots show the results for sixty minutes to be sure that this curve corresponds to steady state. From the steady state curves, the penetration depth of the

therapeutic temperature achievable can be considered to be around 1.5 – 2.0 cm in the worst scenario.

The results shown in Figure 5.14 indicate that the heat removal due to the blood perfusion may produce significant changes in the temperature profile achievable during the treatment. This fact suggests that the effect of blood perfusion should not be neglected and should be included in the simulations. Reliable values for this coefficient for different organs and body regions may be found in literature, for instance see (Kreith F. 2000).

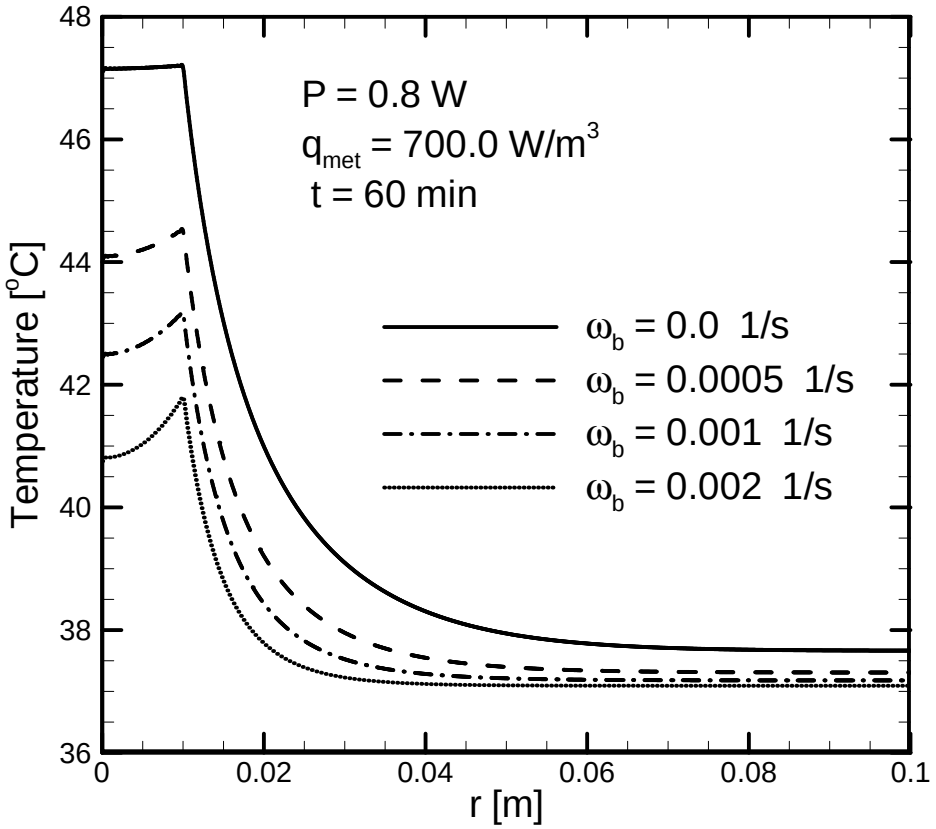

Figure 5.14: Effect of the Blood Perfusion Rate in the Temperature Distribution for a Shell Source

Figure 5.15 shows the temperature profiles for different volume fraction of particles. These particles were assumed to be distributed in a shell of 0.8 mm thickness. The magnetic field intensity and frequency were fixed in the introductory paragraphs at the beginning of this

chapter leading to a linear relationship between the power dissipated and volume fraction. The heating rates under these conditions are shown in Table 5.2. The values for the volume fraction adopted are very close to the typical magnetite dosages of 10 mg of Fe per gram of tumor.

Table 5.2: Heat generation for different volume fraction

Volume fraction	**0.0022**	**0.0026**	**0.0030**	**0.0034**
Source intensity [W]	**0.5983**	**0.7070**	**0.8159**	**0.9245**

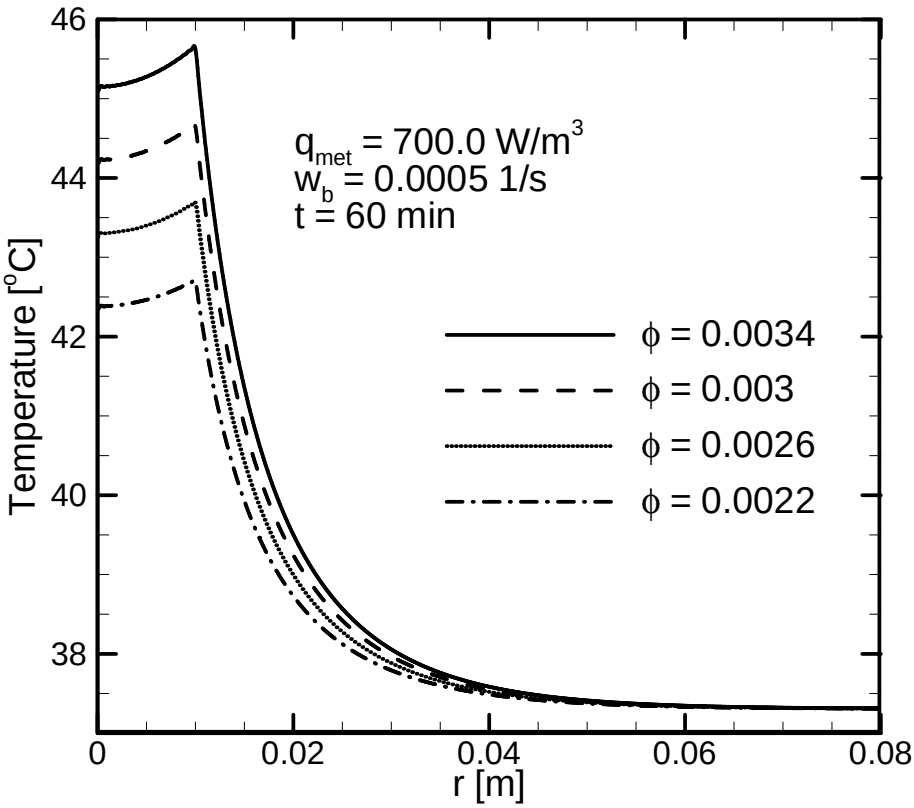

Figure 5.15: Transient temperature profile for a shell source of 0.8 mm thickness and different volume fraction. Outer radius of the shell r_0 = 0.01 m

6 CONCLUSIONS

Several numerical and analytical solutions of Pennes' model (bio-heat equation) were presented in this work.

There was no need to consider the mass diffusion coupled to the heat diffusion because was proven that the time scales are very different being the time scale for the mass diffusion process much higher than that for heat diffusion. This yielded an easier problem to be solved and made the research to be focused in the bio-heat diffusion process.

The Monte Carlo method was shown to be an excellent candidate for bio-heat transfer problems in which the temperature of few isolated points within the domain is required. The method is not efficient for field calculations, even though a coarse grid can be used to get an approximation. The size of the sample must be as large as 5000 random walks in order to get acceptable accuracy.

For field calculations, the finite volume method was used. By integrating the bio-heat equation and performing a discretization a set of linear equations was developed and the Bi-Conjugate Gradient Stabilized solver adapted from literature has shown to be very efficient.

Fundamental or free-space Green's functions have been developed for the bio-heat transfer differential operator in the most used coordinate systems. These are the solution of the differential equation for an unbounded domain such that no particular boundary conditions are used in the solution. These solutions have not been reported in literature yet.

Characteristic sources in each of the commonly used coordinate system were proposed for using the Analytical methods used in this work. These solutions are valuables for getting some insight about the heat diffusion process during the magnetic fluid hyperthermia and

they are also useful for testing numerical codes used for solving problems where complicated geometries and/or sources distribution are present.

The point source solutions showed that the heating rates achievable from a single nanoparticle are not enough to produce the local temperature rise needed in order to reach therapeutic levels.

The solutions suggested that an analysis of the order of magnitude of the heat removed by blood perfusion must be performed. The effects of blood perfusion can considerably reduce the temperature profile and it cannot be neglected; there is no need to consider the variations in the thermo-physical properties of the tissue because they are negligible and do not produce significant modifications in the temperature profile; the profile is steep near the source which traduces in a small penetration depth of the higher temperatures in the tissue; therapeutic values for the temperature were shown to be obtained after 15~20 minutes since the particles start generating heat. This means that if the tumor must be hold in the therapeutic range of temperatures for 30 minutes, the exposure to the magnetic field must be of 45 minutes, at least.

The best temperature profile, *i.e.* the one closest to the ideal, is obtained with a superficial covering of the tumor with the nanoparticles. An almost constant temperature is got inside the domain without penetrating too much the profile in the healthy tissue.

REFERENCES

Andra, W., C. G. d'Ambly, et al. (1999). "Temperature distribution as function of time around a small spherical heat source of local magnetic hyperthermia." Journal of Magnetism and Magnetic Materials **194**: 197-203.

Arkin, H., L. Xu, et al. (1994). "Recent developments in modelling heat transfer in blood perfused tissue." IEEE Trans Biomed Eng **41**: 97–107.

Atkinson, W. J., I. A. Brezovich, et al. (1984). "Usable Frequencies in Hyperthermia with Thermal Seeds." Biomedical Engineering, IEEE Transactions on **BME-31**(1): 70-75.

Bagaria, H. G. and D. T. Johnson (2005). "Transient solution to the bioheat equation and optimization for magnetic fluid hyperthermia treatment." International Journal of Hyperthermia **21**: 57-75.

Beck, J. V., K. D. Cole, et al. (1992). Heat conduction using Green's functions.

C.F. Chan, D., D. B. Kirpotin, et al. (1993). "Synthesis and evaluation of colloidal magnetic iron oxides for the site-specific radiofrequency-induced hyperthermia of cancer." Journal of Magnetism and Magnetic Materials **122**(1-3): 374-378.

Carslaw, H. S. and J. C. Jaeger (1967). Conduction of Heat in Solids, Clarendon Press, Oxford.

Deen (1998), W. Analysis of Transport Phenomena.

Deng, Z.-S. and J. Liu (2002). "Analytical Study on Bioheat Transfer Problems with Spatial or Transient Heating on Skin Surface or Inside Biological Bodies." Journal of Biomechanical Engineering **124**(6): 638-649.

Deng, Z. S. and J. Liu (2002). "Monte Carlo method to solve multidimensional bioheat transfer problem." Numerical Heat Transfer Part B: Fundamentals **42**: 543-567.

Durkee, J. W. and P. P. Antich (1991). "Characterization of bioheat transport using an exact solution of the cylindrical geometry, multi-region, time-dependent bioheat equation." Physics in Medicine and Biology **36**: 1377-1405.

Durkee, J. W. and P. P. Antich (1991). "Exact solutions to the multi-region time-dependent bioheat equation with transient heat sources and boundary conditions." Physics in Medicine and Biology **36**: 345-368.

Durkee, J. W., P. P. Antich, et al. (1990). "Exact solutions to the multiregion time-dependent bioheat equation. I: Solution development." Physics in Medicine and Biology(7): 847.

Durkee, J. W., P. P. Antich, et al. (1990). "Exact solutions to the multiregion time-dependent bioheat equation. II: Numerical evaluation of the solutions." Physics in Medicine and Biology(7): 869.

Erdelyi, A., W. Magnus, et al. (1954). Tables of Integral Transforms. New York, McGraw-Hill.

Ferziger, J. H. and M. Peric (2002). Computational Methods for Fluid Dynamics

Gao, B., S. Langer, et al. (1995). "Application of the time-dependent Green's function and Fourier transforms to the solution of the bioheat equation." Int. J. Hyperthermia **11**: 267–285.

Gilchrist RK, M. R., Shorey WD, Hanselman RC, Parrott JC, Taylor CB. (1957). "Selective inductive heating of lymph." Ann. Surg. **146**: 596 - 606.

Gutierrez, G. (2002). Investigation of Heat Pipes for Drilling Applications, University Of Wisconsin-Milwaukee. **Ph.D.**

Haji-Sheikh, A. Monte Carlo Methods. Handbook of numerical heat transfer, Wiley**:** pp. 673±722.

Hergt, R., W. Andra, et al. (1998). "Physical limits of hyperthermia using magnetite fine particles." IEEE Transactions on Magnetics **34**(5): 3745 - 54.

Jordan, A., R. Scholz, et al. (2001). "Presentation of a new magnetic field therapy system for the treatment of human solid tumors with magnetic fluid hyperthermia." Journal of Magnetism and Magnetic Materials **225**: 118-126.

Jordan, A., R. Scholz, et al. (1999). "Magnetic fluid hyperthermia (MFH): Cancer treatment with AC magnetic field induced excitation of biocompatible superparamagnetic nanoparticles." Journal of Magnetism and Magnetic Materials **201**: 413-419.

Kreith F., T. K., Lior N., Shaw H., Shah R.K., Bell K. J., et al. (2000). The CRC Handbook of Thermal Engineering. E. F. Kreith, CRC Press LLC**:** 114-184.

Moroz, P., S. K. Jones, et al. (2002). "Magnetically mediated hyperthermia: current status and future directions." International Journal of Hyperthermia **18**: 267-284.

Ozisik, M. N. (1968). Boundary Value Problems of Heat Conduction, Dover.

Ozisik, M. N. (1980). Heat Conduction, Wiley & Sons.

Pankhurst, Q. A., J. Connolly, et al. (2003). "Applications of magnetic nanoparticles in biomedicine." Journal of Physics D: Applied Physics(13): R167.

Patankar, S. V. (1980). Numerical Heat Transfer and Fluid Flow

Pennes, H. H. (1948). "Analysis of Tissue and Arterial Blood Temperatures in the Resting Human Forearm." J Appl Physiol **85**(1): 5-34.

Rabin, Y. (2002). "Is intracellular hyperthermia superior to extracellular hyperthermia in the thermal sense?" Int. J. Hyperthermia **18**(3): 194-202.

Rosensweig, R. E. (2002). "Heating magnetic fluid with alternating magnetic field." Journal of Magnetism and Magnetic Materials **252**: 370-374.

Sadiku, M. N. O. (2001). Numerical Techniques in Electromagnetics. Boca Raton, Florida.

Shliomis, M. I. (1974). "Magnetic fluids." Soviet Physics Uspekhi **17**(2): 153-169.

Truskey, G. A., F. Yuan, et al. Transport phenomema in biological systems.

Versteeg, H. and W. Malalasekra (1995). An Introduction to Computational Fluid Dynamics: The Finite Volume Method Jhon Wiley and Sons.

Vyas, R. and M. L. Rustgi (1992). "Green's function solution to the tissue bioheat equation." Medical Physics **19**(5): 1319-1324.

www.nci.nih.gov. "Hyperthermia in Cancer Treatment: Questions and Answers."